Ceramic Strength Models for
Monolithic (isotropic), Transversely-isotropic UD and Fabric Materials

Key-words: UD and fabric ceramics, strength criteria models, model validation by tests

Abstract

Ceramic Material Composites (CMC) are basically used due to their excellent thermomechanical properties at high temperature and resistance again harmful media.
Novel simulation-driven product development requires reliable material models including Strength Failure Criteria (SFC) in order to perform a reliable Design Verification (DV). Thereby, engineering practice demands for a homogeneous macroscopic description of the inhomogeneous composition of constituents and thus aiming at a 'smeared' material. SFC models for such smeared materials are searched which should also capture the failure of its constituents.

The depicted SFCs have been generated by the author's Failure-Mode-Concept (FMC). This incorporates a rigorous thinking in failure modes and can be briefly described by the features: *Failure mode-wise mapping, stress invariant-based formulation, *equivalent stress generation, *each failure mode is just governed by the mode-related strength R^{mode} and eventually, *all SFC model parameters are measurable macroscopic properties. The author's similar Fiber-Reinforced-Plastic (FRP) SFCs were successful in the World-Wide-Failure-Exercises (WWFEs) of Uni-Directional (UD)-composed laminas (plies) and are adapted here for CMC materials.

Material behavior information together with the FMC-based modelling and rendering shall give the necessary understanding for the derivation of the SFCs to be provided for the 3 CMC material model families: Isotropic (monolithic), Transversely-isotropic UD and Woven Fabric.
Model Validation could be performed just for a minimum number of available test data sets from different test specimens composed of UD layers or of fabric layers. These test specimens were coupons and 'filament'-wound tubes (*roving strand-wound*) under different winding angles or were prepreg-'wound' tubes.

Standard uni-axial tests deliver the (scattering) strength test values synonymous for the *uni-axial failure stress* and multi-axial failure stress tests deliver plane (2D) and spatial (3D) failure envelopes required for DV. In order to obtain multi-axial stress states, coupon test specimens are used as uni-axially loaded 'Off-axis' test specimens, possessing different fiber directions, and further above tubes with different winding angles. Possible problems with the evaluation of the test results from the different test specimens will be discussed and enriched by special personal experience collected for FRP materials in the WWFEs etc.

Main conclusions of this private investigation are: *Data sets are missing, *description of the test specimens lacks of clearance such as lay-up and thickness,*test evaluation is not well documented and there was a 'lack of question' regarding those test results which were found critical, *in order to fulfill DV a lot of reliable testing is required in future.
Mapping of the rarely available test data sets with the generated SFCs was successful.

1 Task with Introduction

Continuous fiber reinforced ceramic matrix composites (CMC) are special Composite Materials. CMCs are used in many engineering fields, such as aeronautical, aerospace and automotive, mainly because of their excellent thermomechanical properties at high temperatures and their relatively low density. A Composite Material is a combination of constituent materials, which are different in composition. Its constituents retain their identities in the composite; that is, they do not dissolve or otherwise merge completely into each other although they commonly act. Normally the constituents can be physically identified, and further, there is an interface between them to consider. In this interface, the bonding effectiveness of a weak or strong interphase material is to regard.
The envisaged composite material can hopefully homogenized to a so-called smeared material and thereby becomes optimal for the usually macro-mechanically working design engineer, because this essentially simplifies material modelling, structural analysis and clears the test amount. Basically addressed here are laminated structural components composed of UD and Fabric ceramic materials. For completion, Strength Failure Criteria (SFCs) for the monolithic isotropic CMC are added.

Novel simulation-driven product development shifts the role of physical testing to virtual testing, to simulation, respectively. This requires High Fidelity concerning the material models used. Structural analysis of CMC materials requires a description of the material up to Onset-of-Failure which is fracture failure for the here envisaged brittle CMC-materials and which requires material test-validated SFCs.
In other words, fracture is the Limit State for designing brittle materials. This further means in the case of the very brittle ceramic materials, it is primarily a linear behavior and due to that a relatively simple elastic design task is to face, 'only'. The CMC-Limit State is more-or-less the proportional limit.

Of-course, some non-linearity may come up due to micro-mechanical cracking and debonding of fiber and matrix. If inelastic behavior would be to consider then associated non-linear stress-strain curves were to provide. Such curves represent the evolution of (micro-)damage with increasing loading. This inelasticity might be termed quasi-ductility or quasi-plasticity. In order to capture the multi-axial stress-strain behaviour a so-called *inelastic potential* has to be set up.
Continuum (micro-) Damage Mechanics (CDM) models explain and describe non-linearity of the deteriorating material but do not explicitly predict final failure of a material. Therefore, above SFCs are needed for the prediction of fracture failure as pre-requisite of the structural component's Design Verification (DV).

Resistance of the structural component must be generally demonstrated by a positive Margin of Safety (*MoS*) or a Reserve Factor $RF = MoS - 1 > 1$ in order to achieve Structural Integrity for the envisaged Limit States, see [*CUN22,§12*]!
Nowadays 3D-SFCs become a must regarding the usual 3D FEA stress output. Hence, 3D-SFCs are principally required to firstly perform Design Dimensioning and to finally achieve the Design Verification. The provided SFC are stress-based and not-strain-based. This is rational for brittle materials showing just marginal failure strains.

In the case of brittle materials, a failure body should be presented in order to offer an optimum visualization of the failure behaviour under multi-axial stressing. The surface of such a failure body is determined by the points of all those failure stress state vectors that lead to failure which is here fracture failure.
This surface is mathematically defined by a Failure function F =1 at Onset-of-Failure, which means that 100% of the material strength capacity is reached.

The SFCs, presented and applied in this paper, are those which have been generated by the Failure-Mode-Concept (FMC). The FMC incorporates a rigorous thinking in failure modes and can be briefly described by the features in the abstract. This further involves a novel, because direct use of the material's friction value μ in the case of compressed brittle materials where for instance the FMC model friction *parameter b* can be replaced in the SFC by a complicatedly derived relation to the measurable friction *value* delivering *μ(b), see [CUN22,§7]*.

Presented are SFC models for monolithic, UD lamina and fabric lamina ceramics. This includes 3D- and 2D-stress state-dedicated SFCs. Basic focus here is the in-plane shear τ_{WF} influence of the fabric CMC.
These stress-based SFCs are chosen because one has to follow the traditional DV procedure using authority-accepted 'strength Design Allowables'. Also residual stresses can be simply imported in the case of stress-based SFCs but not in the case of strain-based ones.

Experience of the author, see [*Cun08, Cun17*], gave him the knowledge that FMC-based SFCs which worked for similar behaving materials can be applied for CMC, too.

Model Validation is performed on basis of the above mentioned different test specimens. Thereby the desire for the testing is: Approximate 'as built' as good as possible!

2 Ceramic UD and Fabric Materials and their Mechanical Properties

2.1 Short Description of Ceramic Materials

Ceramic material is an inorganic, metallic oxide, nitride, silicon, aluminum oxide or carbide material. Some elements, such as carbon or silicon, may be considered ceramics. Usually they are brittle, hard, relatively strong in compression, and weak in shearing and tension. They are applied if wear and high temperature are faced and are characterized by chemical resistance and corrosion resistance. The material properties are fully linked to the manufacturing process steps, see figure below. Decisive for the CMC material properties in the structural component are type, frequency and distribution of flaws, pores.

A common application example is C/C-SiC, which is manufactured under shielding gas from silicon and carbon powder and which has a fracture strain of about 0.5% (*extracted from [Sch23] and - Information for us structural engineer readers).*

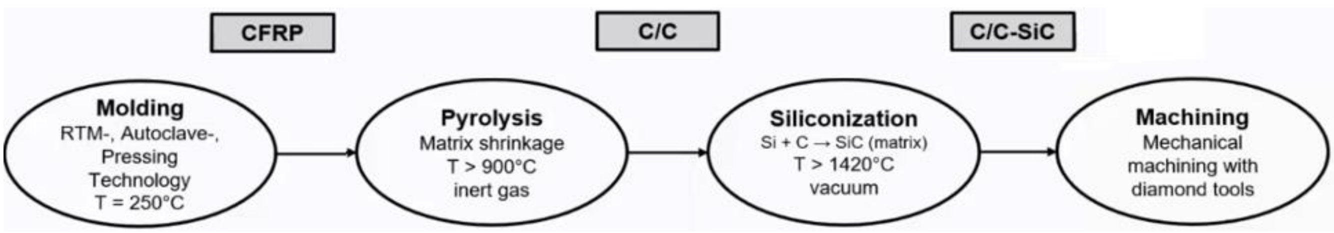

Scheme of the exemplary process Liquid Siliconization ([Sch23])

2.2 Solid Mechanical Description of Ceramic Material Models and Terms

In order to use a 'clear' wording and nouns in *Fig.1* the 3D stress states applied for the three ceramic material model families are depicted. For fabrics, it was helpful that a different English

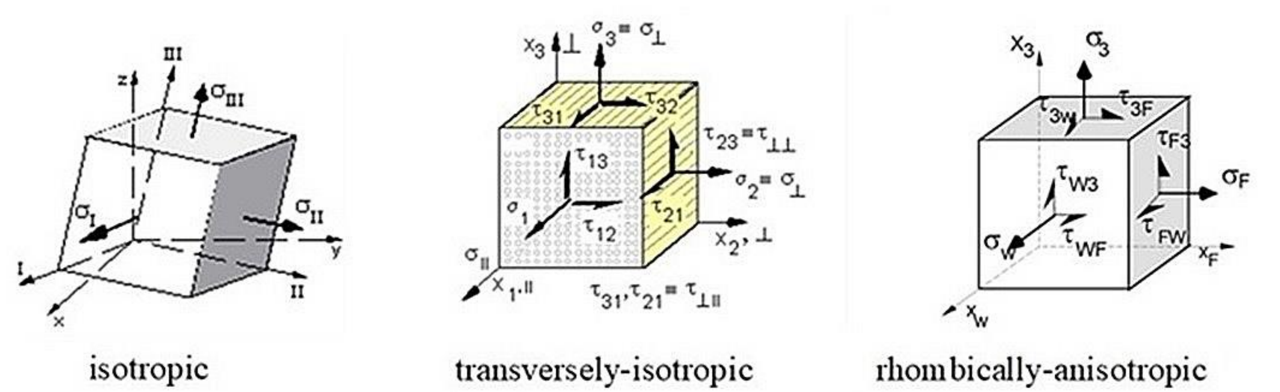

$\{\sigma\} = (\sigma_x, \sigma_y, \sigma_z, \tau_{yz}, \tau_{xz}, \tau_{xy})^T$ $\quad$ $\{\sigma\} = (\sigma_1, \sigma_2, \sigma_3, \tau_{23}, \tau_{13}, \tau_{21})^T$ $\quad$ $\{\sigma\} = (\sigma_W, \sigma_F, \sigma_3, \tau_{3F}, \tau_{3W}, \tau_{FW})^T$

Isotropic: $\{R\} = (R^t, R^c)^T$ with μ

Transversely-isotropic: $\{R\} = (R_{\parallel}^t, R_{\parallel}^c, R_{\perp}^t, R_{\perp}^c, R_{\perp\parallel})^T$ with $\mu_{\perp\parallel}, \mu_{\perp\perp}$

Orthotropic: $\{R\} = (R_W^t,\ R_W^c,\ R_F^t,\ R_F^c,\ R_{WF},\ R_3^t,\ R_3^c,\ R_{3F},\ R_{3W})^T$ with $\mu_{WF}, \mu_{3W}, \mu_{3F}$

Fig.1: 3D-stress states and strengths employed in ceramic analyses Warp (W, Kette), Fill (F, Schuss, weft). Rhombically-anisotropic = orthotropic

index $_F$ could be found for Weft [*VDI2014*] namely Fill and thereby avoid confusion with the equal index $_W$ for Warp. Pointed out are the descriptions of the stresses and the strengths to insert into SFCs. The figure represents a simplification which is helpful for the structural modeler.

To be introduced now is the so-called 'material stressing effort' in the relationship $\sigma = R \cdot Eff$, which later will be employed. This is an artificial term, generated in the WWFE in order to get an English term for the meaningful German term Werkstoffanstrengung.

In this paper the envisaged laminates are built of UD and fabric materials. There are UD-layer- and fabric layer-based semi-finished ceramic products which – again - require a very different modeling that affords a right lay-up description.

An urgent point for a reliable structural modelling is a clear description of the specific laminate used for the laminated wall. Laminates can be composed of single UD-layers and of layers built by semi-finished products like the stitched Non-Crimp-Fabrics (NCF) or by woven fabrics like plain weave or the various satin (atlas) versions. These different building-blocks or sub-laminates of a laminate behave differently and this is of highest interest for the mechanical modeler and the test evaluation engineer. Hence, always required is a 'clear' lay-up (stack) description of ceramic UD, NCF and Fabric materials and that all relevant mechanical properties are listed.

Fig.2 depicts available semi-finished products. They are separated into so-called 'closed' ones and 'open' ones, like the reinforcing fiber grids in civil engineering. Whether fiber grids might be of interest for distinct ceramic applications is not yet discussed, [*CUN,§3*].

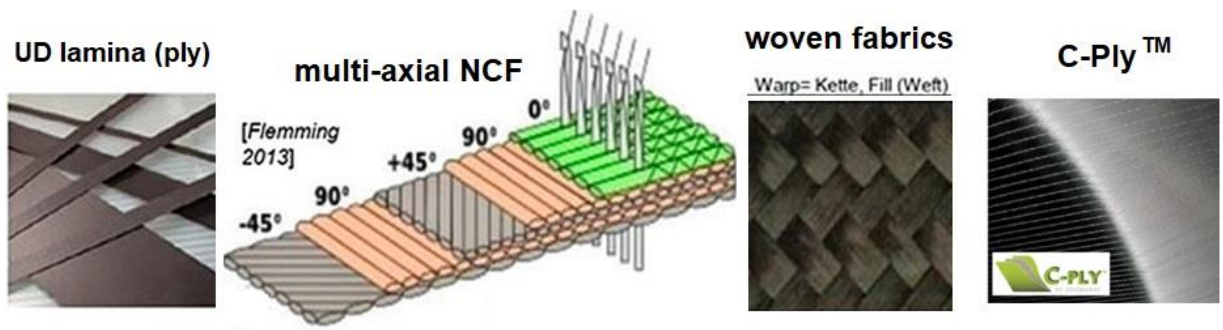

Fig.2, Visualization of applicable closed fiber reinforcing semi-finished products:(left) UD-layer (ply), composing traditional laminates, stitched Non-Crimped Fabrics (NCF) and woven fabric, (right) novel deliverable C-ply^{TM} = balanced angle ply (see [*Cun23a*]

The description of a UD-lamina-composed laminate follows the well-known lay-up denotation $[0/90/90/0] = [0/90]_S$, and an angle-ply laminate is denoted $[45/-45]_S$ with index $_S$ for symmetric (*targeting coupling reduction in [K]).* Analogously follows for a symmetrically stacked woven satin fabric $\begin{bmatrix} 0 \\ 90 \end{bmatrix}_S$ (*plain weave, that is symmetric in itself*) or for an angle-ply semi-finished product $[\pm 45]_S$**.** The survey below shall visualize by some examples how one can distinguish the various types. Square bracket [ ] and wavy bracket { } optically help here to distinguish NCF **{**stitched UD-stack**}** from those woven fabrics where one practically cannot mechanically separate the single woven layers within one fabric layer:

Single UD-layers-*deposited* stack $[0/90]_S = [0/90/90/0]$-lay-up

Semi-finished product, *stitched* NCF: $\{0/90\} + \{90/0\}$ symmetrically stacked

deliverable 'building blocks' $\{0/45/\text{-}45/90\}$, novel C-ply™ $\{\varphi/\text{-}\psi/\text{-}\varphi/\psi\}$ etc.

Semi-finished product, *woven* Fabric: $\begin{bmatrix} 0 \\ 90 \end{bmatrix}_S = \begin{bmatrix} 0 \\ 90 \end{bmatrix}_2$.

In the context above it is to define: Technical strengths are the uni-axial normal failure stresses under tension and compression. The shear strength practically is a bi-axial failure stress which is to consider in the SFC approaches. Regarding for instance UD-stresses, there are to distinguish <u>inter-laminar</u> stresses $\{\sigma\} = (0,0,\sigma_3,\tau_{23},\tau_{31},0)^T$ and in-plane-working <u>intra-laminar</u> stresses $\{\sigma\} = (\sigma_1,\sigma_2,0,0,0,\tau_{21})^T$. The *inter-laminar* stresses are basically the reason for delamination.

For rounding the understanding of the body text, <u>*Table 1*</u> presents the compliance matrices which include the elasticity properties required in design and needed in test data evaluation. The stress-strain relations of the investigated UD and fabric material families are depicted by the following two compliance matrices.

Table 1: UD- and fabric compliance matrices for test data evaluation

$\{\varepsilon\} = [S] \cdot \{\sigma\}$ with $[S]$ compliance matrix, $\{\sigma\} = [C] \cdot \{\varepsilon\}$ with $[C]$ stiffness matrix

$$[S] = \begin{bmatrix} \frac{1}{E_\parallel} & \frac{-\nu_{\parallel\perp}}{E_\perp} & \frac{-\nu_{\parallel\perp}}{E_\perp} & 0 & 0 & 0 \\ \frac{-\nu_{\perp\parallel}}{E_\parallel} & \frac{1}{E_\perp} & \frac{-\nu_{\perp\perp}}{E_\perp} & 0 & 0 & 0 \\ \frac{-\nu_{\perp\parallel}}{E_\parallel} & \frac{-\nu_{\perp\perp}}{E_\perp} & \frac{1}{E_\perp} & 0 & 0 & 0 \\ & & & \frac{1}{G_{\perp\perp}} & 0 & 0 \\ & \text{(symm.)} & & & \frac{1}{G_{\perp\parallel}} & 0 \\ & \boxed{\text{transversely isotropic}} & & & & \frac{1}{G_{\perp\parallel}} \end{bmatrix} \qquad [S] = \begin{bmatrix} \frac{1}{E_W} & \frac{-\nu_{WF}}{E_F} & \frac{-\nu_{W3}}{E_F} & 0 & 0 & 0 \\ & \frac{1}{E_F} & \frac{-\nu_{F3}}{E_F} & 0 & 0 & 0 \\ & & \frac{1}{E_3} & 0 & 0 & 0 \\ & \text{(symm.)} & & \frac{1}{G_{F3}} & 0 & 0 \\ & \boxed{\text{orthotropic (also called rhombically anisotropic)}} & & & \frac{1}{G_{W3}} & 0 \\ & & & & & \frac{1}{G_{WF}} \end{bmatrix}.$$

Due to thermodynamic reasons the compliance matrix must be symmetric. This means in case of transversely-isotropic materials that the following condition of Maxwell-Betti $\nu_{\perp\parallel} \cdot E_\perp = \nu_{\parallel\perp} \cdot E_\parallel$ is valid. In contrast to many codes, here ν_{21}, ν_{FW} are the larger Poisson ratios *(this is the old and more logic notation, which was forever used for loadings!)* and the lines 6 and 4 are not changed in the compliance matrices as it is sometimes done!

Deriving SFCs, on basis of the author's FMC, means to effectively use demands coming from material symmetry. <u>*Table 2*</u> below comprises a very interesting result, namely, that there seems to

Table 2: Material symmetry-based scheme indicating the 'generic' numbers [Cun23a]

Isotropic Material: **'generic' numbers 2 and 1**
- **2** e*lastic 'constants' E, ν; 2 strengths; 2 strength failure modes fracture* (NF, SF); *2 modes yielding* (Normal Yielding NY, Shear Yielding SY); etc.
Ductile: 1 stress-strain curve due to SY, $R^t_{0.2} = R^c_{0.2}$; a so-called flow potential captures multi-axial behavior.
Brittle: 2 stress-strain curves due to NF, SF; a so-called inelastic potential captures multi-axial behavior.
- **1** *physical parameter CTE, CME, μ, etc.)*
Transversely-Isotropic Material: **'generic numbers 5 and 2**
- **5** e*lastic 'constants', 5 strengths, 5 strength failure modes fracture* (NF, SF), 5 stress-strain curves
- **2** *physical parameters (CTE, CME, $\mu_{\perp\perp}$ $\mu_{\perp\parallel}$ etc.)*
Orthotropic Fabric Material: **' generic numbers 9 and 3**
- 9 e*lastic 'constants', 9 strengths, 9 strength failure modes fracture* (NF, SF)
- *3 physical parameters (CTE, CME, μ etc.).*

be a 'generic' number for above three material 'families'. This information is essential for simplifying material modeling and testing. From this number it can be concluded "More properties need not to be measured than this number demands". Beside the strengths, friction occurs under compressive stress conditions due to the validity of Mohr-Coulomb *(a real material is not internally friction-free like the ideal crystal*).

Exemplarily for a fabric, 3 material friction values must be used for the general 3D-stressed fabric in addition to the 9 strengths, namely μ_{WF}, μ_{W3}, μ_{F3} and are to be measured, see [*CUN§2*].

Especially for CMC fabrics is valid:

If Fill = Warp (F ≡ W) only 6 values have to be determine) instead of the general 9 entities
6 strengths : $R_W^t = R_F^t$, $R_W^c = R_F^c$, R_{WF}, R_3^t, R_3^c, $R_{3W} = R_{3F}$
6 elastic entities : $E_W = E_F$, E_3, G_{WF}, $G_{W3} = G_{F3}$, ν_{WF} , $\nu_{W3} = \nu_{F3}$ and
2 friction values remain: μ_{WF}, $\mu_{W3} = \mu_{F3}$.

2.3 Stress-strain behavior and Failure Behavior

In rare cases (*Save the Design*) a non-linear analysis might be necessary. This requires the full stress-strain curve capturing hardening and softening and the choice of an 'inelastic potential' for combining multiaxial stresses with the strains. For the envisaged very brittle ceramic matrix just the hardening domain is significant for practical engineering applications.

UD materials show 5 clear failure modes, woven fabrics practically do not.

Not very clear and scattering mode-related strength measurement results are observed. Therefore, the strengths have to be defined according to the number of material symmetry demands for orthotropic fabrics, the generic number gives guidance.

The different effect of so-called 'isolated' stress-controlled (→ *measured strengths*) and strain-controlled embedded layers in the case of brittle matrices is marginal because the present porosity partly decouples the multi-axial stress states.

Usable knowledge regarding failure and measurement: Fiber undulation causes bending stresses. In this context as still mentioned, for most of the fabrics fractography will not exhibit clear failure modes. In these materials always multiple micro-cracking is caused under tension, compression, bending, or shear. Under a (macro-scopic) compressive stress, the fabric is generally subject to inherent micro-crack tensile failure (*due to internal local 3D-stress states*) and to micro-instability in free, not well embedded or not mutually supports fiber bundles in the porous material.

Internal friction in CMC materials is different to the transversely-isotropic UD FRP material, and measurement is more complex. Simplifying consideration: As a number for practical application on the 'safe side' shall be given following the present knowledge of the author: $\mu_{\perp\perp} = \mu_{\perp||} = 0.15$, $\mu_{WF} \approx \mu_{W3} = \mu_{F3} = 0.3$.

2.4 Fabric Specifica

To quantify the always present differences between R_W^t and R_F^t or R_W^c and R_F^c, test specimens in both the directions W and F are equally (*i.e. plain weave fabric*) to produce and statistically to test (50% each), so that the necessary information in both the fiber directions is obtained. Under shear τ_{WF}, the shear stress-shear strain curve continues to rise after initial fracture, because the so-called scissor effect causes a rearrangement in the direction of fibers, which means the originally 90°-angle of the fabric becomes smaller.

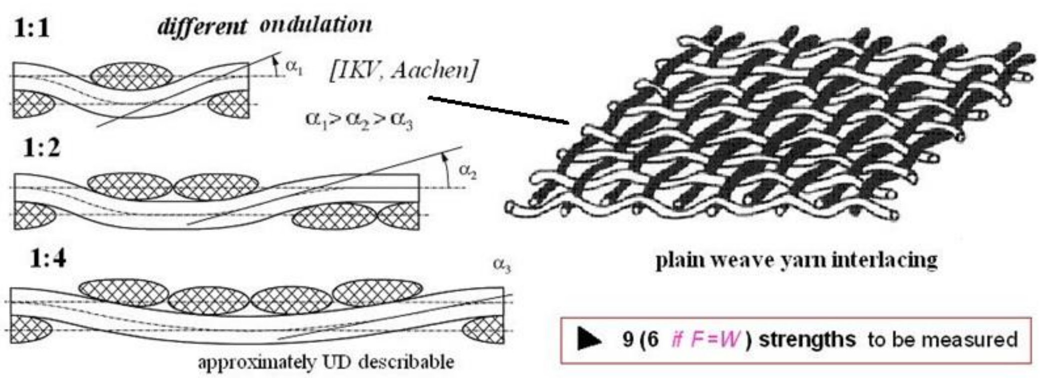

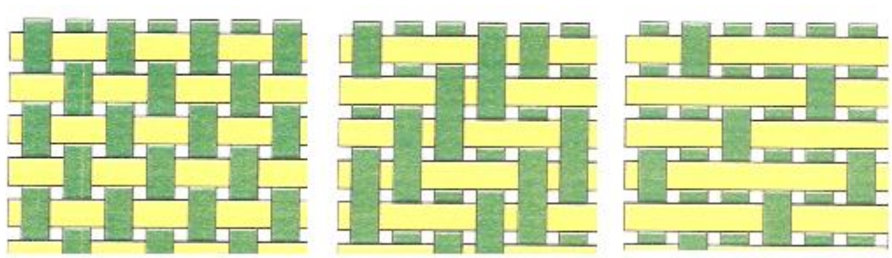

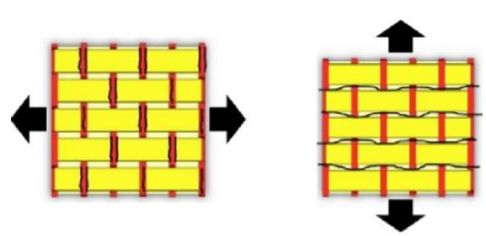

Fig.3: (up) Differently woven fabrics [IKV Aachen]. (center) Plain weave (Leinwandbindung) → Twill weave (Köperbindung) 2/2 → Atlas or Satin weave1/4 [Wikipedia 2023]; (down) Different fracture failure due to ceramic pockets impacting progressive failure

Fig.3 visualizes different fabrics. The upper part figure depicts the modelling of differently woven fabrics, the center shows three basic fabrics, and the bottom part figure fabric 'pocket' effects. The pockets with their porosity impact the progressive micro-damage under orthogonal uni-axial tensile stress states. Under compression, the above still mentioned micro-instability is faced. Differently woven means different fracture failure due to the ceramic pockets.
Pocket-driven supported fracture failure is desired if some quasi-ductility is to provide.

3 Uni-axial and Multi-axial Strength Testing

3.1 General

Failure behavior of composite materials has to be investigated under different loading conditions to activate different multi-axial stress states. Special focus is directed to the in-plane behavior to get a more detailed picture of the intra-laminar deformation and associated failure behavior. Dealing with flat structural components requires test specimens cut from flat plates, since these come closest to 'as built' of the later composite component. Thus, tube test specimens are usually excluded in those cases, but taken if for the design of rotationally–symmetric components properties of a cylinder, a dome a centrifuge or a nozzle are to provide.

For the choice and sometimes the necessary design of such test specimens some prerequisites are given:

1. In the critical locations of the test specimen a distinct size of a homogeneous, uniform stress state domain with no other stresses should be present to clearly transfer the failure stress state into a uniaxial strength or a multi-axial strength envelope
2. A test data set is principally just valid for the applied geometry of the test specimen, the rate of displacement and the test temperature
3. Similarity of the manufactured specimen's material and the material in the structural component is the more valid for composite ceramic materials (see *point 2.*)
4. If applied, then 'Thin'-walled and 'Thick'-walled Tube Tests require different, careful evaluation.

The uni-axial test specimens, coupon and 90°tube (*about 88° in reality due to roving band width*), serve for tensile and compressive strength determination. Differences between tensile and compressive test specimens come from the necessity to stabilize by a buckling device.

It is natural, that different values can be obtained using different procedures to estimate strength, especially shear strength, as different micro-damage mechanisms are activated in each test type used for the experimental determination of a property value. Standards help to reduce this scatter of results and offer a basis for a common definition to enable a comparison of the results and finally determine a reliable strength value for design.

Unfortunately in CMC material development works, often test data is just 'found' for bending and Inter-Laminar-Shear-Strength (ILSS) as production quality entities. However, in-plane properties are to provide for design, too.

The test effort is always linked to the necessity to realistically represent the stress conditions occurring during real world service.

3.2 Coupon Testing employing Tension, Compression and Shear

The determination of the in-plane (intra-laminar) and out-of-plane (inter-laminar) shear properties (strength, strain and moduli) of flat laminate sheet materials is of great interest, and many different testing procedures have been developed within the last decades to attempt to generate the needed data. The UD 10°-off-axis test specimen in *Fig.4* was attributed in 1977 [*Cha77*] by C. Chamis and J. Sinclair to be a convenient test method for the in-plane-shear characterization but it has its limits.

In order to obtain the strengths of UD and Fabric materials ‘dogbone-shaped’ coupon test specimens are used, as shown in *Fig.4. These i*nclined (oblique) tests are executed to investigate combinations of normal stress with shear stress or multi-axial failure stress states, respectively. These tests are so called “off-axis tests” which unfortunately exhibit the so-called edge effect (*see a later note for detail*).

The off-axis test has its problems to deliver the desired realistic strength results, because these values significantly depend on the complete fixture in the test rig. It is to prevent: splitting, fracture failure within the tab domain, using oblique end-tabs and rotating grips to obtain an optimal gripping in the inclined case of test specimen.

It is practice for CMC tests to use higher angles (15°, 30°, 45°) in order to obtain a higher shear stress to normal stress ratio and to investigate the stress-strain behavior associated micro-damage increase. This makes to check the width, proving that fibers are not running through from one end to the other.

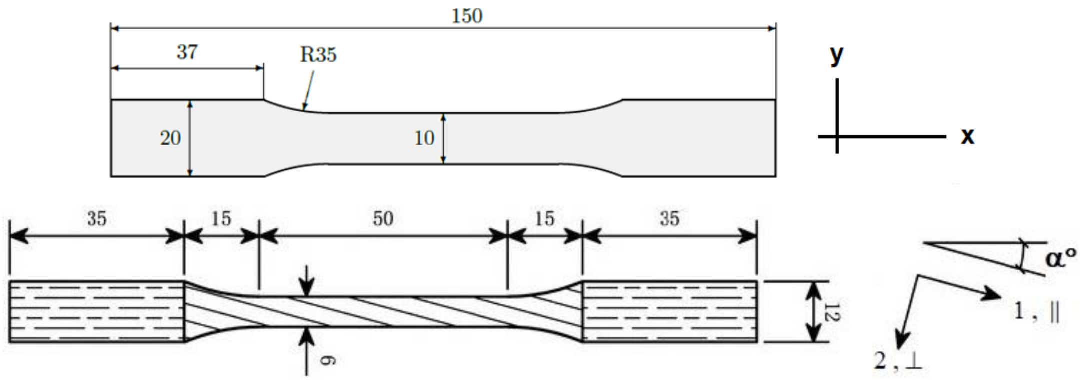

Fig.4, front views: (up) Dogbone-shaped test specimen after ASTM- or EU-standard. Structural coordinate system (CoS , x, y) and material coordinate system (CoS fabric F, W and CoS UD 1≡ ||, 2≡ ⊥). (down) 10°-tensile test specimen (Chamis-Sinclair proposal 1977)

A tension test of a $[45/-45)_S$-laminate is one of the most used techniques to determine by CoS transformation the UD shear modulus value (*less good for strength*). ASTM D 3518, EN 6031 allow a laminate of just 8 plies.

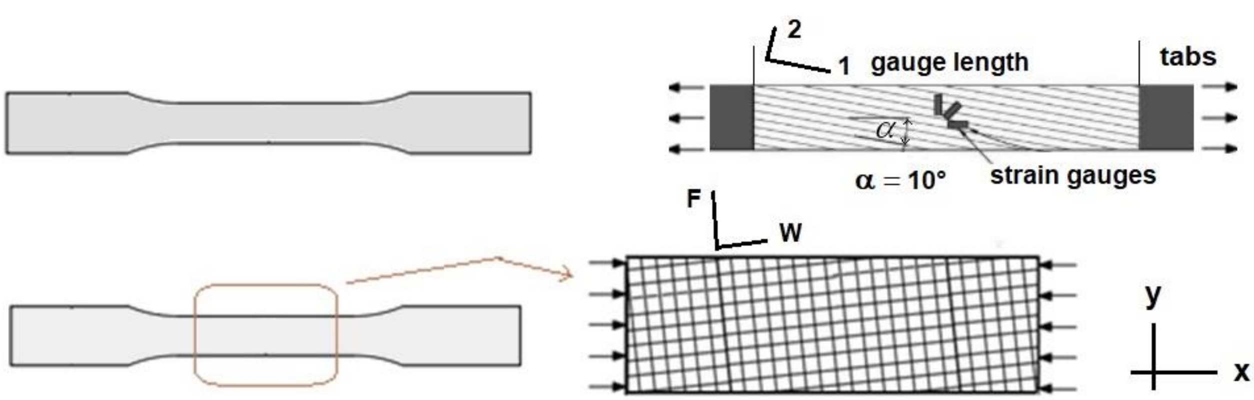

Fig. 5 Typical dogbone coupon test specimens:(up) Off-axis coupon tensile UD test specimen,. (down) the shorter $\begin{bmatrix}0\\90\end{bmatrix}_S$ *fabric coupon compression test specimen*

A tension test of a $[45/-45]_S$-laminate is one of the most used techniques to determine by CoS transformation the UD shear modulus value (*less good for strength*). ASTM D 3518, EN 6031 allow a laminate of just 8 plies.

Fig.5 displays some dogbone-shaped coupon test specimens, showing a width reduction of the dogbone in the foreseen fracture domain. More realistic strength results for UD test specimens are given by tapering the thickness and not reducing the width *(tests of H. Schürmann at TU Darmstadt and H. Bansemir at Airbus*, Ottobrunn).

A problem with the off-axis coupon test specimen is the significant free edge effect. Although this is not as with a polymer matrix UD laminate, e.g. the laminate [0/90/90/0], the stress rising edge effect from the unequal deformation of 0°-layer and the neighbor 90°-layer but in this even more brittle CMC fabric laminate a consequence of the many natural defects at the free edge. The consequence is that τ must grow within the length of the laminate thickness from zero up at the edge to the in-plane value. Hence, smaller strength values are applied. The edge effect can be theoretically considered with the method of Finite Fracture Mechanics [*Met23*].

Fig.6 depicts the off-axis equilibrium in a fabric test specimen example under a single-axial stress $\sigma_x = \sigma_{ax}$ where σ_F is complementary to σ_W. At an angle of 45°, the cutting stresses σ_W and σ_F are of the same size on both cutting surfaces, detail in *Fig.6.* At around 15° an internal, micromechanical stress state occurs, where the matrix is stressed the highest and which leads to matrix fracture failure (*see chapter 5*).

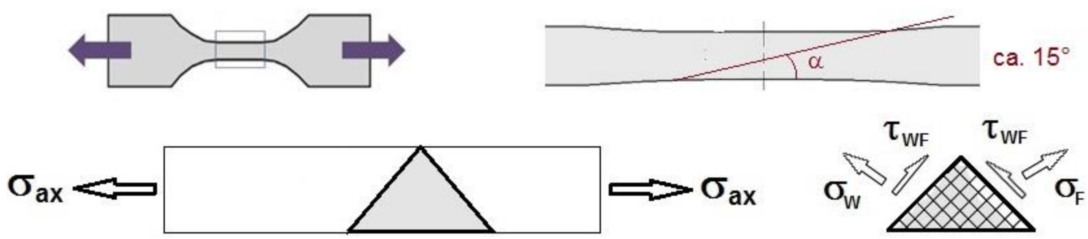

Fig.6: Determination of σ_W (τ_{WF}), or complementary of σ_F (τ_{WF}), equilibrium in the test specimen under a uni-axial stress $\sigma_x = \sigma_{ax}$

The relationships of the stresses, regarding the fiber orientation angle α, read

$$\{\sigma'\} = (\sigma_x, \sigma_y, \tau_{xy})^T = [T_\sigma]\cdot\{\sigma\}, \quad \rightarrow \quad \{\sigma\} = (\sigma_W, \sigma_F, \tau_{WF})^T = [T_\sigma]^{-1}\cdot\{\sigma'\},$$

$$\begin{Bmatrix} \sigma_W \\ \sigma_F \\ \tau_{WF} \end{Bmatrix} = \begin{bmatrix} c^2 & s^2 & 2sc \\ s^2 & c^2 & -2sc \\ -sc & sc & c^2 - s^2 \end{bmatrix} \cdot \begin{Bmatrix} \sigma_x \\ 0 \\ 0 \end{Bmatrix}; \quad c = \cos\alpha = \cos(\alpha° \cdot \pi / 180°)$$

Applying the equations above it become:

$\sigma_W = c^2\cdot\sigma_x$ and σ_F are complementary (not in the same section) and $\tau_{WF} = 2\cdot s\cdot c\cdot\sigma_x$.

Two numerical examples shall explain the stress situation in the inclined cutting cross section.

The structural stress state, loading a usually symmetrically stacked $[45/\text{-}45]_S$ UD test specimen or a $\begin{bmatrix} +45 \\ -45 \end{bmatrix}_S$ fabric test specimen reads $\{\sigma\} = (\sigma_x = 100,\ \sigma_y = 0,\ \tau_{xy} = 0)^T$, laminate thickness 1mm. This structural stress state in the structural CoS (x,y) is to transform into the UD or the Fabric material CoS (W,F) for each layer of the laminate. A numerical example shall visualize the procedure by some data..

UD $[45/\text{-}45]_S = [45/\text{-}45/\text{-}45/45]$:

2D-tensile loaded in the 4 single layers the stresses are (*shear stress is computed like above*):

Plane stress state reads

$$\rightarrow \{\sigma\} = (\sigma_x = 100, \sigma_y = 0, \tau_{xy} = 0)^T = (\sigma_1, \sigma_2, 0\ ,0\ ,0\ ,0.5 \cdot \sigma_x)^T = (70.7,\ 29.3\ ,0\ ,0\ ,0\ ,\pm 50)^T \text{MPa}$$

Fabric $\begin{bmatrix} 0 \\ 90 \end{bmatrix}_S$ plain weave:

2D-tensile loaded under an angle 45° identical to a 0°-tensioned 45°-cut out test specimen:

$$\rightarrow \{\sigma\} = (\sigma_x = 100, \sigma_y = 0, \tau_{xy} = 0)^T \rightarrow \quad (\sigma_W, \sigma_F, 0\ ,0\ ,0\ ,\tau_{WF})^T = (50, 50\ ,0\ ,0\ ,0\ ,\pm 50)^T \text{ MPa.}$$

3.3 Tube Testing employing Tension, Compression and Shear

If a Tension/Compression-Torsion test (T/C-T) device is available then tubes can be produced with different winding angles, analogous to the inclined coupon test specimen.

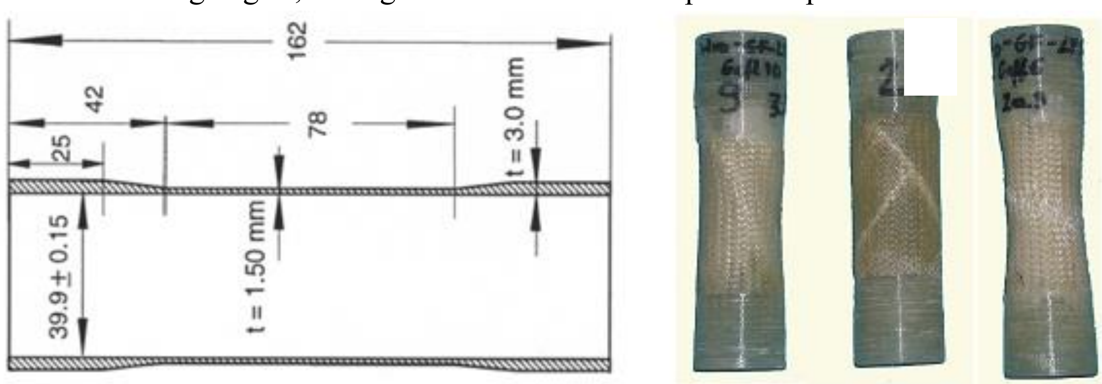

Fig.7: Tension/compression-torsion (T/C-T) tube test specimen, 90°-filament winding (UD) and tube failures. Hoop is 90° fiber direction (used at MAN-Technologie in many projects especially for data gaining for uranium enrichment centrifuges, see [CUN,§19]). Tube test specimens can be applied to all 3 families. Tube testing can be performed by the T/C-T device in the interaction zone compressive stress - shear stress and this delivers the friction value

If a laminate test specimen is not symmetrically built up the coupon warps and the tube turns. Facing these effects makes the evaluation of test results difficult. Tube specimens have the drawback of its cost and needing above device.

In this context, remembering the WWFEs, the contributing author likes to mention Lessons Learned from test data interpretation of differently derived test sets: (1) [*WWFE-I, TC2, plane stress states*], here the author informed the organizers that apples and oranges have been put together in a diagram. One cannot fill into the same diagram 90°-wound tube test specimen data together with 0°-wound tube data. The 0°-stresses have to be transformed in the 2D-plane due to the fact that shearing under torsion loading (see Fig.7) turns the fiber direction and the lamina CoS is not anymore identical with the structural CoS of the tube. In order to also use the 0°-test data set the author transformed the fracture test point data by the occurring twisting angle using a non-linear CLT-analysis. Then he could achieve a good mapping of both the data sets in the lamina CoS. (2) [*WWFE-II, TC3, 3D stress states*], the same mistake happened again, but there the much more complicated 3D-stress situation was to face, the 3D-transformation of the 0°-data set was very complicated but successfully carried out as mapping proved. *See [Cun13, CUN§6]).*

3.4 Iosipescu Shear Testing, ASTM D5379

For measuring the pure shear strength Iosipescu-test specimen is used, depicted in *Fig.8*. The Josipescu shear test is a V-notched short beam test. A shear loading rate of 1 mm/min is used at Siemens AG test lab from where some fabric fracture test data could be obtained and investigated in a later chapter. Chosen was a layup of several fabric plies leading to a mm-specimen thickness, cut out of a thick UD panel.

In [*Kum02*) it has been shown for woven fabrics that the shear strength from the Iosipescu shear test is significantly higher than the shear strength from the traditional $(45/-45)_S$-tensile specimen tests and that the initiation of in-plane micro-damage in the tensile specimen still occurs at lower loads than with the Iosipescu test specimen (*Fig.8*) in the Iosipescu test device. For the author exist two reasons: The so-called edge effect with its singularities and, further, that in the Iosipescu test specimen the domain of highest shear stress is restricted to the center which means to a smaller volume of overstressing (*Weibull volume effect*). The occurring strain behavior, depicted in the figure, has been determined by means of digital image correlation (DIC). The region of interest is in the central part where pure shear deformation is predicted by means of FE analysis.

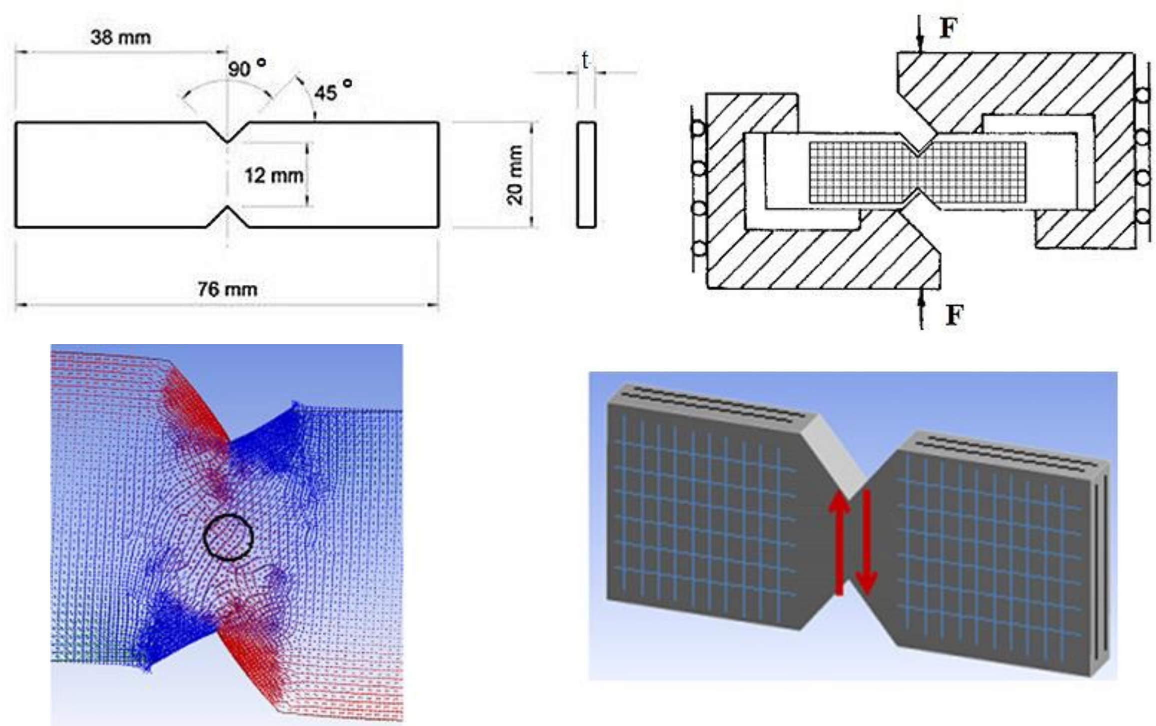

Fig.8: (up) V-notched-shear test specimen [Siemens AG] and loading fixture of Iosipescu test specimen. (below) FEA shear stress field from [Pet15]and loaded test specimen

3.5 Coupon Test Specimens for Fabric Ox/Ox strength evaluation

The investigated CMC off-axis test specimens (at Siemens AG) consist of an oxide matrix and an oxide fiber. The matrix is based on aluminum oxide slurry. For the fiber reinforcement, a Nextel 610 fiber 8H-satin weave has been chosen. In this 8H satin weave binding pattern the fill yarn floats *over* seven warp yarns and *under* one warp yarn. It is the most pliable satin weave and forms well around curved part surfaces of a structural component. The test specimen is built up from **12** woven fabric layers resulting in a thickness of about 2.4 mm and involving a fiber volume ratio of about V_f = 40%, *see Fig.9*. The geometry of the test specimens for the in-plane tension and the compression tests in 0°, 15°, 30° and 45° loading direction (*measured from the warp as 0°-direction to the fill direction*) follows the DIN EN 658-1 and the ASTM C1275. The inclined test specimens are produced via a beam laser by cutting them out of the manufactured CMC plates (*courtesy: Siemens, T. Steinkopf)*. The shape of the test specimen types, indicated by the off-axis loading angle 15°, 30° and 45°, is shown in *Fig.9*.

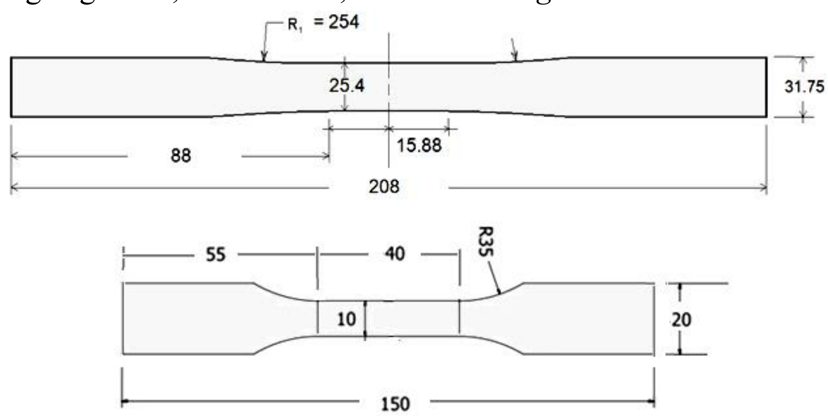

Fig.9 Dogbone-shaped-test specimen: $\begin{bmatrix} 0 \\ 90 \end{bmatrix}_{12}$, *t = 2.4* mm, fabric *Nextel 610 fiber 8H-satin weave.*
(up) Tension, (down) Compression [*courtesy Siemens AG*]

For all the compression tests wider and shorter dimensions are necessary and a buckling device is necessary to avoid any buckling. In this context, the Standards are thereby helpful tools to obtain comparable test results for Design Dimensioning and design values for the Design Verification. The shape of the test specimen follows practical pre-requisites, such as the individual material challenges.

4 Modelling of Macro-mechanical Strength Failure applying Cuntze's Failure Mode Concept

4.1 General

Engineers prefer macro-mechanical models in order to design on the usual macro-scopic design level, which is also the usual FE output. This also marks the procedure in Cuntze's Failure-Mode-Concept FMC. The basic features of the FMC are:

- ***Each failure mode represents 1 independent failure mechanism,***
  and thereby represents 1 piece of the complete failure surface or failure body
- ***Each failure mechanism is governed by 1 basic strength*** *(this is witnessed)*
- ***Each failure mode can be represented by 1 strength failure condition SFC.***
  Therefore, equivalent stresses can be computed for each mode.
- Consequently, this modal approach requires the interaction of all modes!

$$Eff = \sqrt[m]{(Eff^{\text{mode 1}})^m + (Eff^{\text{mode 2}})^m + \ldots} = 1 = 100\%\,,\ \ if \quad \text{Onset of Failure}$$

Above interaction of the adjacent failure modes is modelled by a 'series failure system". That permits to formulate the total material stressing effort from all activated failure modes as an 'accumulation' of *Effs* ≡ sum of all the failure danger proportions of the laminas in the laminate,

Eff = 1 mathematically represents the surface of a failure body.

- The value of the interaction exponent m depends a little on the ratio R^c / R^t with its scatter. From engineering reasons, Cuntze takes the same interaction exponent m for each transition zone between failure mode domains. For brittle materials with about $R^c / R^t > 3$ the value is about $m = 2.6$ from mapping experience in the transition zones of modes. A smaller m is 'design verification conservative'.

Most of the traditional SFCs are formulations that mathematically map test data courses crossing different failure modes. One might call this type of SFCs the so-called 'global fitting' ones. However, for the designing engineer is decisive that there is a basic physical difference between a 'global fitting' one (*traditional SFCs of Drucker-Prager, Tsai-Wu, Willam-Warnke, Altenbach etc.*) and a failure mode-linked 'modal fitting' one, similar to the successful 'Mises Yield SFC' for ductile materials. In order to discriminate SFCs the author choose the term "Global" as a 'play on words' to "modal" and hopes both the terms are being self-explaining names, [*Cun§2*].

The collected knowledge about the materials leads in the FMC to:

1. A rigorous postulation of a number of failure modes = number of strengths
2. Application of a failure mode-wise concept for the generation of SFCs
3. A direct use of the friction value μ in the SFCs and
4. All model parameters, strengths and friction values, can be measured.

Two effects are considered in contrast to the traditional SFCs:

Mixed Strength (fracture) Failure: Different failure modes may be activated by the acting stress state. The interaction of both the activated fracture mode types Normal Fracture NF with Shear

Fracture SF under compression increases the danger to fail! Hence, the associated fracture test data are so-called joint-probabilistic results of two acting modes!

Multi-fold (fracture) Failure Mode: An acting in-plane stress state with maximally equal orthogonal stresses activates the same mode two-fold. Hence, the associated fracture test data are so-called joint-probabilistic results of a two-fold acting mode!

Modelling of ceramic laminates may be lamina-based (basic layers are UD layers), sub-laminate-based (semi-finished non-crimp orthotropic fabrics) or even laminate-based. Thereby, modelling complexity grows from UD, via non-crimp fabrics through plain weave and finally to the spatial 3D-textile materials.

4.2 Isotropic Monolithic Material

For completion, the SFCs for the monolithic model shall be added, see *Table 3*. These SFCs must capture the porosity ρ, the size of which depends on the grade of porosity and determines the choice of the SFC. It is valid

$$\bar{R}^{c} < \bar{R}^{cc} \text{ (not so porous, } \rho) \quad \text{or} \quad \bar{R}^{c} > \bar{R}^{cc} \text{ (very porous, similar to foam).}$$

The bar in SFC marks that for modeling the average behavior the average strength is to apply, which is denoted in statistics by the bar over. $\bar{R}^{cc}$ represents the bi-axial compressive failure stress.

There are some facts to consider:

- Spatial ceramic fracture stress data is not available
- The investigation of *Fig.13* will prove that the mapping of the course of test data points will decide on the SFC choice → therefore, two different SFCs will be provided, visualized by similarly behaving materials where test data sets were available
- Isotropic materials possess a 120°-rotationally symmetric failure body, see [*Cun23a*].

Table 3a shows the full analytical procedure "*How the failure body is to obtain*".

According to the fact "Spatial ceramic fracture stress data is not available" for the isotropic-modeled monolithic ceramics and according to the author's experience, the relately-behaving material 'light concrete' is used to visualize the formulas.

On the fracture failure body figure below the 3 main meridians are outlined. For the tensile meridian a Lode angle ϑ = +30° is valid and for the compressive meridian -30°. The shear meridian was chosen by the author as neutral meridian with a Lode angle ϑ = 0. For each mode, the SFC model parameters must be determined in each associated 'pure' failure mode domain.

To remember is: *bi-axial tension = 'weakest link failure behavior* and *bi-axial compression = redundant (benign) failure behavior, but this depends on the fact whether the solid is 'dense' and not fully porous like the special foam later.*

Table 3a: Strength Failure Criteria (SFC) for the Isotropic marginal porous ceramic material

* Normal Fracture NF for $I_1 > 0$ $\Leftarrow$ SFCs $\Rightarrow$ Shear Fracture SF for $I_1 < 0$

$$F^{NF} = c^{NF} \cdot \frac{\sqrt{4J_2 \cdot \Theta^{NF} - I_1^2/3} + I_1}{2 \cdot \bar{R}^t} = 1 \quad \leftrightarrow \quad F^{SF} = \frac{c_{2\Theta}^{SF} \cdot I_1}{\bar{R}^c} + c_{1\Theta}^{SF} \cdot \frac{3J_2 \cdot \Theta^{SF}}{(\bar{R}^c)^2} = 1$$

after inserting $\sigma = R \cdot Eff$ and dissolving for Eff follows

$$Eff^{NF} = c^{NF} \cdot \frac{\sqrt{4J_2 \cdot \Theta^{NF} - I_1^2/3} + I_1}{2 \cdot \bar{R}^t} = \frac{\sigma_{eq}^{NF}}{\bar{R}^t} \leftrightarrow Eff^{SF} = \frac{c_{2\Theta}^{SF} \cdot I_1 + \sqrt{12J_2 \cdot c_{1\Theta}^{SF} \cdot \Theta^{CrF} + (c_{2\Theta}^{SF} \cdot I_1)^2}}{2 \cdot \bar{R}^c} = \frac{\sigma_{eq}^{CrF}}{\bar{R}^c}.$$

with $I_1 = (\sigma_I + \sigma_{II} + \sigma_{III}) = f(\sigma)$, $6J_2 = (\sigma_I - \sigma_{II})^2 + (\sigma_{II} - \sigma_{III})^2 + (\sigma_{III} - \sigma_I)^2 = f(\tau)$

$$27J_3 = (2\sigma_I - \sigma_{II} - \sigma_{III}) \cdot (2\sigma_{II} - \sigma_I - \sigma_{III}) \cdot (2\sigma_{III} - \sigma_I - \sigma_{II}).$$

If a failure body is rotationally symmetric, then $\Theta = 1$ like for the neutral or shear meridian, respectively . A 2-fold acting mode makes the rotationally symmetric fracture body 120°-symmetric and is modelled by using the invariant J_3 and Θ as non-circularity function with d as non-circularity parameter

$$\Theta^{NF} = \sqrt[3]{1 + d^{NF} \cdot \sin(3\vartheta)} = \sqrt[3]{1 + d^{NF} \cdot 1.5 \cdot \sqrt{3} \cdot J_3 \cdot J_2^{-1.5}} \quad \leftrightarrow \quad \Theta^{SF} = \sqrt[3]{1 + d^{SF} \cdot 1.5 \cdot \sqrt{3} \cdot J_3 \cdot J_2^{-1.5}}$$

Lode angle ϑ , here set as $\sin(3 \cdot \vartheta)$ with ‘neutral‘ (shear meridian) angle $\vartheta = 0°$ ($\rightarrow \Theta = 1, d = 0$) ;

tensile meridian angle 30° $\rightarrow \Theta^{NF} = \sqrt[3]{1 + d^{NF} \cdot (+1)}$; compr. mer. angle -30° $\rightarrow \Theta^{SF} = \sqrt[3]{1 + d^{SF} \cdot (-1)}$.

Mode interaction $\rightarrow$ Equation of the fracture body: $Eff = [(Eff^{NF})^m + (Eff^{SF})^m]^{m^{-1}} = 1 = 100\%$

$$Eff = \sqrt[m]{(c_{1\Theta}^{NF} \cdot \frac{\sqrt{4J_2 \cdot \Theta^{NF} - I_1^2/3} + I_1}{2 \cdot \bar{R}^t})^m + (\frac{c_{2\Theta}^{SF} \cdot I_1 + \sqrt{12J_2 \cdot c_{1\Theta}^{SF} \cdot \Theta^{SF} + (c_{2\Theta}^{SF} \cdot I_1)^2}}{2 \cdot \bar{R}^c})^m} = 1.$$

* 120°-rotat. symmetric $\Theta \neq 1$:

$c_{1\Theta}^{NF} \rightarrow c^{NF} = 1$ ($\Theta^{NF} = 1$ in practice chosen). $c_{2\Theta}^{SF} = (1 + 3\mu)/(1 - 3\mu)$ from [CUN §5].

$c_{1\Theta}^{NF}, d^{NF}$ from the 2 points $(\bar{R}^t, 0, 0) \rightarrow c_{1\Theta}^{NF}$ and $(\bar{R}^{tt}, \bar{R}^{tt}, 0) \rightarrow d^{NF}$ or min.error fit of data course

$c_{1\Theta}^{SF}, d^{SF}$ from the 2 points $(-\bar{R}^c, 0, 0) \rightarrow c_{1\Theta}^{SF} = 1 + c_{2\Theta}^{SF}$ and $(-\bar{R}^{cc}, -\bar{R}^{cc}, 0) \rightarrow d^{SF}$.

The failure surface is closed at the upper end, a paraboloid serves as closing cap

$$\frac{I_1}{\sqrt{3} \cdot \bar{R}^t} = s^{cap} \cdot (\frac{\sqrt{2J_2 \cdot \Theta^{NF}}}{\bar{R}^t})^2 + \frac{\max I_1}{\sqrt{3} \cdot \bar{R}^t} .$$

The slope parameter s is determined connecting the respective hydrostatic strength point $\max I_1$ with the associated point on the tensile meridian. $\max I_1$ must be assessed,[CUN §5].

The bottom end is not closed if the material is dense, like the present one.

The ‘material stressing effort’ above works analogous to ‘Mises’

$$Eff^{\text{yield mode}} = \sigma_{eq}^{\text{Mises}} / R_{0.2} \rightarrow Eff^{\text{fracture mode}} = \sigma_{eq}^{\text{fracture mode}} / R .$$

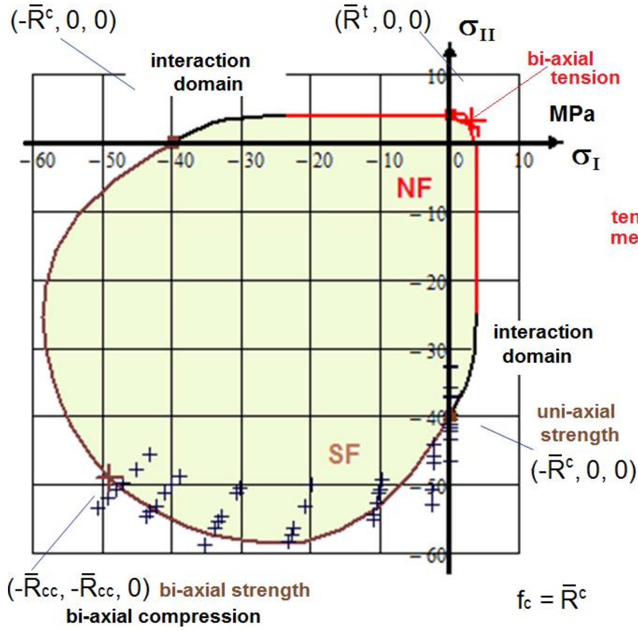

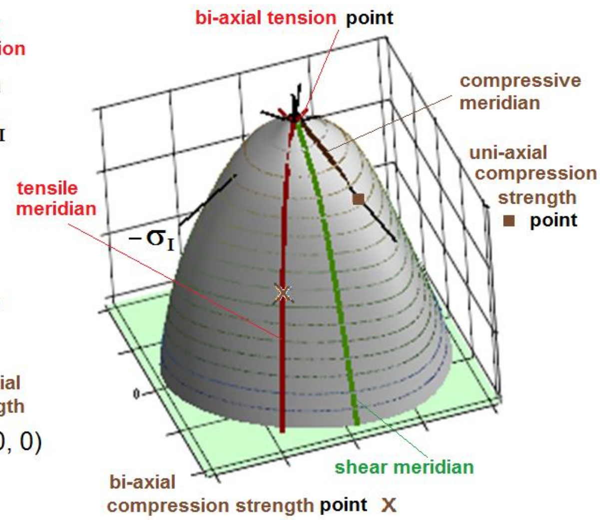

$$Eff = (Eff^{NF})^m + (Eff^{SF})^m = 1$$

Fig.10: Normal Concrete, mapping of 2D-test data in the Principal Stress Plane (bias cross-section of fracture body). R:= strength; t:=tensile, c:=compressive; bar over means mean value. μ = 0.2. (test data, courtesy Dr. S. Scheerer, IfM Dresden). See [*CUN22,§5.4*]

$\bar{R}^t = 4$ MPa, $\bar{R}^c = 40$ MPa, $\bar{R}^{tt} = 0.8 \cdot \bar{R}^t$ (assumed) = 3.2, $\bar{R}^{ttt} = 2.81$, $\bar{R}^{cc} = 49$ MPa,
$\bar{R}^{ccc} = 1000$ MPa (set, necessary for computation), $\max I_1 = 8.43$; $\min I_1 = -4.58$, $m = 2.5$
120°-rotationally-symmetry parameter: $c^{SF}_{1\Theta} \cdot \Theta^{SF} = 1 + c^{SF}_{2\Theta}$ with $c^{SF}_{2\Theta}$ as friction parameter
$c^{NF} = 0.86$, $d^{NF} = 0.86$, $c^{SF}_{2\Theta} = 0.26$, $c^{SF}_{1\Theta} = 1.04$, $d^{SF} = 0.13$, $\Theta^{SF} = 0.51$, $s^{cap} = -1.31$.

For interest is, which failure modes might be activated by a single shear stress or a single normal stress:

$*\tau_{xy}$: a shear stress activates 2 fracture failure modes

$$Eff^{\text{fr}} = \sigma^{\text{fr}}_{eq} / \bar{R}^t: \quad \tau_{xy} \rightarrow I_1 = 0,\ J_2 = \tau_{xy}{}^2;\ \ \sigma_x \rightarrow I_1 = \sigma_x,\ J_2 = \sigma_x{}^2/3. \quad c_1^{SF} = 1 + c_2^{SF}$$

$$\rightarrow \sigma^{\text{NF}}_{eq} = 1 \cdot (\sqrt{4J_2 \cdot 1 - I_1{}^2/3} + I_1)/2;\ \ \sigma^{\text{SF}}_{eq} = (c_2^{SF} \cdot I_1 + \sqrt{(c_2^{SF} \cdot I_1)^2 + 12 \cdot c_1^{SF} \cdot J_2 \cdot 1})/2$$

and the relations read $\tau_{xy} \rightarrow \sigma^{\text{NF}}_{\text{eq}} = 1 \cdot \tau_{xy}$ and $\sigma^{SF}_{eq} = \sqrt{3} \cdot \tau_{xy}$.

$*\ \sigma_x$: a normal tensile stress actives either NF or SF

$$\rightarrow \sigma^{NF}_{eq} = 1 \cdot \sigma_x,\ \sigma^{SF}_{eq} = 0.5 \cdot \sigma_x \cdot \sqrt{c_2^{SF\,2} + 4 \cdot (1 + c_2^{SF}) \cdot 1}.$$

The other similarly behaving material is a very porous foam. *Table 3b shows "How the foam's failure body is to obtain".*

Simplifying the failure body of brittle isotropic materials by choosing a rotationally symmetric *fracture* failure body model - as it is performed with the 'Mises' *yield* cylindrical body - the SFCs are displayed in *Table 3c*.

Table 3b: Strength Failure Criteria (SFC) for the Isotropic porous ceramic material

* Normal Fracture NF for $I_1 > 0$ $\Leftarrow$ SFCs $\Rightarrow$ Crushing Fracture CrF for $I_1 < 0$

$$F^{NF} = c_\Theta^{NF} \cdot \frac{\sqrt{4J_2 \cdot \Theta^{NF} - I_1^{\,2}/3} + I_1}{2 \cdot \bar{R}^t} = 1 \quad \leftrightarrow \quad F^{CrF} = c_\Theta^{CrF} \cdot \frac{\sqrt{4J_2 \cdot \Theta^{CrF} - I_1^{\,2}/3} + I_1}{2 \cdot \bar{R}^c} = 1$$

after inserting $\sigma = R \cdot Eff$ and dissolving for Eff follows

$$Eff^{NF} = c_\Theta^{NF} \cdot \frac{\sqrt{4J_2 \cdot \Theta^{NF} - I_1^{\,2}/3} + I_1}{2 \cdot \bar{R}^t} = \frac{\sigma_{eq}^{NF}}{\bar{R}^t} \leftrightarrow Eff^{CrF} = c_\Theta^{CrF} \cdot \frac{\sqrt{4J_2 \cdot \Theta^{CrF} - I_1^{\,2}/3} + I_1}{2 \cdot \bar{R}^c} = \frac{\sigma_{eq}^{CrF}}{\bar{R}^c}.$$

with $I_1 = (\sigma_I + \sigma_{II} + \sigma_{III}) \;=\; f(\sigma)$, $6J_2 = (\sigma_I - \sigma_{II})^2 + (\sigma_{II} - \sigma_{III})^2 + (\sigma_{III} - \sigma_I)^2 = \; f(\tau)$

$$27J_3 = \; (2\sigma_I - \sigma_{II} - \sigma_{III}) \cdot (2\sigma_{II} - \sigma_I - \sigma_{III}) \cdot (2\sigma_{III} - \sigma_I - \sigma_{II}).$$

If a failure body is rotationally symmetric, then $\Theta = 1$ like for the neutral or shear meridian, respectively. A 2-fold acting mode makes the rotationally symmetric fracture body 120°-symmetric and is modelled by using the invariant J_3 and Θ as non-circularity function with d as non-circularity parameter

$$\Theta^{NF} = \sqrt[3]{1 + d^{NF} \cdot \sin(3\vartheta)} = \sqrt[3]{1 + d^{NF} \cdot 1.5 \cdot \sqrt{3} \cdot J_3 \cdot J_2^{\,-1.5}} \quad \leftrightarrow \quad \Theta^{CrF} = \sqrt[3]{1 + d^{CrF} \cdot 1.5 \cdot \sqrt{3} \cdot J_3 \cdot J_2^{\,-1.5}}$$

Lode angle ϑ , here set as $\sin(3 \cdot \vartheta)$ with 'neutral' (shear meridian) angle $\vartheta = 0°$ ($\rightarrow \Theta = 1, d = 0$) ;

tensile meridian angle 30° $\rightarrow \Theta^{NF} = \sqrt[3]{1 + d^{NF} \cdot (+1)}$; compr. mer. angle -30° $\rightarrow \Theta^{CrF} = \sqrt[3]{1 + d^{CrF} \cdot (-1)}$.

Mode interaction $\rightarrow$ Equation of the fracture body: $Eff \; = [(Eff^{NF})^m + (Eff^{CrF})^m]^{m^{-1}} = 1 = 100\%$

$$Eff \;=\; \sqrt[m]{(c_{1\Theta}^{NF} \cdot \frac{\sqrt{4J_2 \cdot \Theta^{NF} - I_1^{\,2}/3} + I_1}{2 \cdot \bar{R}^t})^m + (c_\Theta^{CrF} \cdot \frac{\sqrt{4J_2 \cdot \Theta^{CrF} - I_1^{\,2}/3} + I_1}{2 \cdot \bar{R}^c})^m} = 1.$$

* 120°-rotat. symmetric $\Theta \neq 1$:

$c_\Theta^{NF} \rightarrow c^{NF} = 1$ ($\Theta^{NF} = 1$ in practice chosen).

c_Θ^{NF}, d^{NF} from the 2 points $(\bar{R}^t, \; 0, \; 0) \rightarrow c_\Theta^{NF}$ and $(\bar{R}^{tt}, \bar{R}^{tt}, \; 0) \rightarrow d^{NF}$ or min.error fit of data course

c_Θ^{CrF}, d^{CrF} from the 2 points $(-\bar{R}^c, \; 0, 0) \rightarrow c_\Theta^{CrF}$ and $(-\bar{R}^{cc}, -\bar{R}^{cc}, 0) \rightarrow d^{CrF}$.

The failure surface is closed at both the ends! A paraboloid serves as closing cap and bottom

$$\frac{I_1}{\sqrt{3} \cdot \bar{R}^t} = s^{cap} \cdot (\frac{\sqrt{2J_2 \cdot \Theta^{NF}}}{\bar{R}^t})^2 + \frac{\max I_1}{\sqrt{3} \cdot \bar{R}^t} \quad , \quad \frac{I_1}{\sqrt{3} \cdot \bar{R}^t} = s^{bot} \cdot (\frac{\sqrt{2J_2 \cdot \Theta^{CrF}}}{\bar{R}^t})^2 + \frac{\min I_1}{\sqrt{3} \cdot \bar{R}^t}$$

Slope parameters s are determined connecting the respective hydrostatic strength point with the associated point on the tensile and compressive meridian, $\max I_1$ must be assessed whereas $\min I_1$ can be measured. $\bar{R}^t$ works as normalization strength. $[CUN\,§5]$).

Fig.11 presents the visualization of the foam SFC in Table 3b. The full data set is added.

Table 3c: 2D SFCs for low and high porous ceramic materials. $\Theta = 1$

$$Eff^{NF} = \frac{\sqrt{4J_2 - I_1^2/3} + I_1}{2\cdot \bar{R}^t} \leftrightarrow Eff^{CrF} = c^{CrF}\cdot \frac{\sqrt{4J_2 - I_1^2/3} + I_1}{2\cdot \bar{R}^c} \quad \text{high porous}\cdot$$

$$Eff^{NF} = \frac{\sqrt{4J_2 - I_1^2/3} + I_1}{2\cdot \bar{R}^t} \leftrightarrow Eff^{SF} = \frac{c_2^{SF}\cdot I_1 + \sqrt{(c_2^{SF}\cdot I_1)^2 + 12\cdot c_1^{SF}\cdot 3J_2\cdot 1}}{2\cdot \bar{R}^c},\; c_1^{SF} = 1 + c_2^{SF}.$$

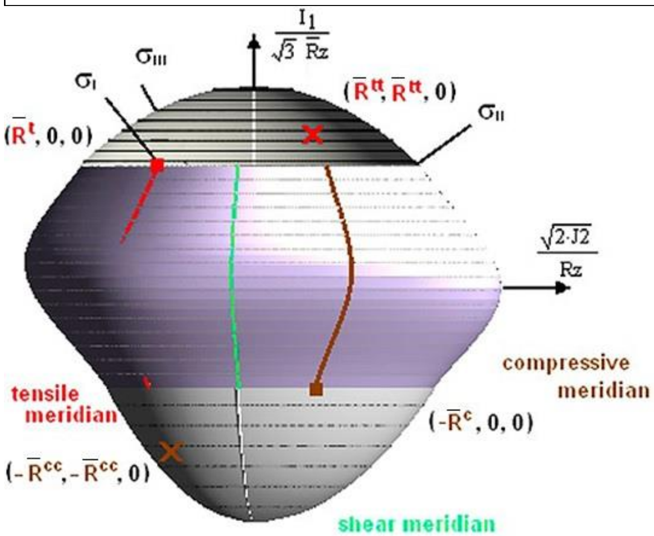

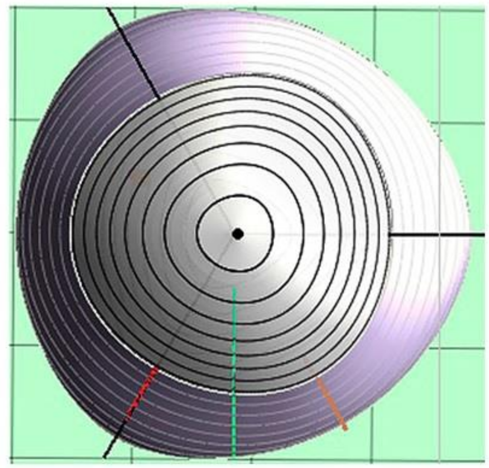
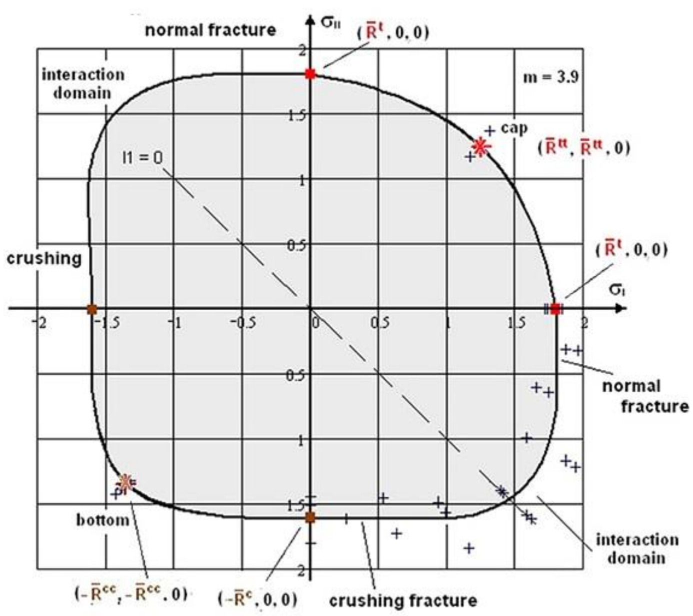

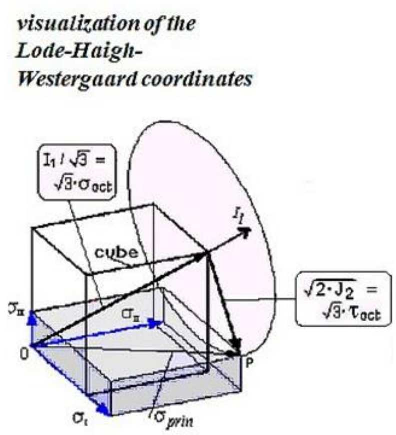

Fig.11, Rohacell 71 IG: Fracture body with its different meridians (left) and view from top (right). The test points are located at a distinct Lode angle of its associated ring o, 120°-symmetry.
Foam Rohacell 71 IG: Mapping of 2D-test data in the Principal Stress Plane.
MathCad plot [test data: courtesy V. Kolupaev, LBF Darmstadt]

$$\bar{R}^t = 1.8;\; \bar{R}^{tt} = 1.25;\; \bar{R}^{ttt} = 1.01;\; \bar{R}^c = 1.65;\; \bar{R}^{cc} = 1.4;\; \bar{R}^{ccc} = 1.53,\; \max I_1 = 3.03;$$
$$\min I_1 = -4.58,\; d^{NF} = -0.71;\; d^{CrF} = 0.21;\; c^{CrF} = 1.03, s^{cap} = -0.27;\; s^{bot} = 0.87,$$
$$\vartheta^{NF} = -0.57;\; \vartheta^{CrF} = 0.52; \Theta^{NF} = 1.2;\; \Theta^{CrF} = 1.07, m = 2.5.$$

Cap and bottom are closed by a cone shape, a shape, being on the conservative side.

4.3 Transversely-isotropic UD Material

Table 4 provides the FMC-derived 5 SFC formulations for porous UD ceramics. The applied invariants stem from [*Boe85*]

$$I_1 = \sigma_1,\ I_2 = \sigma_2 + \sigma_3,\ I_3 = \tau_{31}{}^2 + \tau_{21}{}^2,\ I_4 = (\sigma_2 - \sigma_3)^2 + 4 \cdot \tau_{23}{}^2,$$
$$I_5 = (\sigma_2 - \sigma_3) \cdot (\tau_{31}{}^2 - \tau_{21}{}^2) - 4\tau_{23}\tau_{31}\tau_{21},$$

The invariants are replaced in the following SFCs directly by their defining lamina stresses. The computation follows the Classical Laminate Theory CLT.

Table 4 'porous' UD materials: SFC formulations for all 5 modes FF1, FF2 and IFF1, IFF2, IFF3

FF1: $Eff^{\|\sigma} = \sigma_1 / \bar{R}_{\|}^{t} \quad = \sigma_{eq}^{\|\sigma} / \bar{R}_{\|}^{t}$

FF2: $Eff^{\|\tau} = -\sigma_1 / \bar{R}_{\|}^{c} \quad = +\sigma_{eq}^{\|\tau} / \bar{R}_{\|}^{c}$

IFF1: $Eff^{\perp\sigma} = 0.5 \cdot [(\sigma_2 + \sigma_3) + \sqrt{\sigma_2{}^2 - 2\sigma_2 \cdot \sigma_3 + \sigma_3{}^2 + 4\tau_{23}{}^2}\,] / \bar{R}_{\perp}^{t} \quad = \sigma_{eq}^{\perp\sigma} / \bar{R}_{\perp}^{t}$

IFF2: $F_{porosity}^{SF} = 0.5 \cdot \sqrt{a_{\perp\perp por}{}^2 \cdot I_2{}^2 + b_{\perp\perp por}{}^2 \cdot I_4} - a_{\perp\perp por} \cdot I_2 \ ] \ / \bar{R}_{\perp}^{c} = 1$

FF3: $Eff^{\perp\|} = \{0.5 \cdot [b_{\perp\|} \cdot I_{23-5} + (\sqrt{b_{\perp\|}{}^2 \cdot I_{23-5}{}^2 + 4 \cdot \bar{R}_{\perp\|}{}^2 \cdot (\tau_{31}^2 + \tau_{21}^2)^2}\,] / \bar{R}_{\perp\|}{}^3\}^{0.5}$.

$\{\sigma_{eq}^{\text{mode}}\} = (\sigma_{eq}^{\|\sigma},\ \sigma_{eq}^{\|\tau},\ \sigma_{eq}^{\perp\sigma},\ \sigma_{eq}^{\perp\tau},\ \sigma_{eq}^{\|\perp})^T$, $I_{23-5} = 2\sigma_2 \cdot \tau_{21}^2 + 2\sigma_3 \cdot \tau_{31}^2 + 4\tau_{23}\tau_{31}\tau_{21}$.

Insertion: Compressive strength point (0, $-\bar{R}_{\perp}^{c}$) + bi-axial fracture stress $\bar{R}_{\perp}^{tt}$ (porosity effect)

delivers $a_{\perp\perp por} \cong \mu_{\perp\perp} / (1 - \mu_{\perp\perp})$, $b_{\perp\perp por} = a_{\perp\perp por} + 1 = 1/(1 - \mu_{\perp\perp})$, $b_{\perp\|} \cong 2 \cdot \mu_{\perp\|}$.

From mapping experience obtained typical FRP-ranges: $0 < \mu_{\perp\|} < 0.3$, $0 < \mu_{\perp\perp} < 0.2$.

From the few CMC test results, due to *Fig*.15, it is recommended $\mu_{\perp\|} < 0.3$.

Failure Surface (failure body) = interaction equation for porous UD ceramics:

$Eff^{m} = (Eff^{\|\tau})^m + (Eff^{\|\sigma})^m + (Eff^{\perp\sigma})^m + (Eff^{\perp\tau})^m + (Eff^{\perp\|})^m = 100\%$ if failure

Two-fold failure danger in the σ_2-σ_3-domain stands for a failure surfce closing, modelled by

$Eff^{m} = (Eff^{\|\tau})^m + (Eff^{\|\sigma})^m + (Eff^{\perp\sigma})^m + (Eff^{\perp\tau})^m + (Eff^{\perp\|})^m + (Eff_{\perp}^{\text{MfFd}})^m = 1$

with $Eff_{\perp}^{\text{MfFd}} = (\sigma_2^t + \sigma_3^t) / 2\bar{R}_{\perp}^{tt}$, and $\bar{R}_{\perp}^{tt} \approx \bar{R}_{\perp}^{t} / \sqrt[m]{2}$ after [*Awa78*]

considering $\sigma_2^t = \sigma_3^t$ and $\sigma_2^c = \sigma_3^c$; $\bar{R}_{\perp}^{tt} \le \bar{R}_{\perp}^{t}$, $\bar{R}_{\perp}^{cc} \le \bar{R}_{\perp}^{c}$ if porous.

From mapping experience obtained typical range of interaction exponent $2.5 < m < 2.9$.

As conditions for the laminate delamination failure a *subset* of the 5 SFCs above with the index $_3$ can be used.

The interaction equation includes all mode material stressing efforts, and each of them represents a portion of load-carrying capacity of the material. If the total *Eff* becomes > 100% then the Eff^{mode} values indicate in which mode or modes the design screw has to be turned via re-design in order to lower the respective Eff^{modes}. Resulting negative signs for Eff are physically wrong, an effort can be only positive. This is formalistically to by-pass by using the Macauly

brackets (≡ Föppl symbols {}) of the equations in order to achieve a fully automatic numerical procedure.
For in-plane loading, the by-passing looks like below:

$$\{\sigma\}=(\sigma_1,\sigma_2,\tau_{12})^{\mathrm{T}}, \quad \{\bar{R}\}=(\bar{R}_{\|}^{t},\bar{R}_{\|}^{c},\bar{R}_{\perp}^{t},\bar{R}_{\perp}^{c},\bar{R}_{\perp\|})^{T}, \ \mu_{\perp\|}.$$

$$Eff=[(Eff^{\|\sigma})^m+(Eff^{\|\tau})^m+(Eff^{\perp\sigma})^m+(Eff^{\perp\|})^m+(Eff^{\perp\tau})^m]^{m^{-1}}$$

$$Eff^{\|\sigma}=\frac{(\sigma_1+|\sigma_1|)\cdot E_{\|}}{2\cdot R_{\|}^{t}}, \ Eff^{\|\tau}=\frac{(-\sigma_1+|\sigma_1|)\cdot E_{\|}}{2\cdot R_{\|}^{c}}, \ Eff^{\perp\sigma}=\frac{\sigma_2+|\sigma_2|}{2\cdot\bar{R}_{\perp}^{t}}, \ Eff^{\perp\tau}=\frac{-\sigma_2+|\sigma_2|}{2\cdot\bar{R}_{\perp}^{c}}, \ Eff^{\perp\|}=\frac{|\tau_{21}|}{\bar{R}_{\perp\|}+0.5\cdot\mu_{\perp\|}\cdot(-\sigma_2+|\sigma_2|)}$$

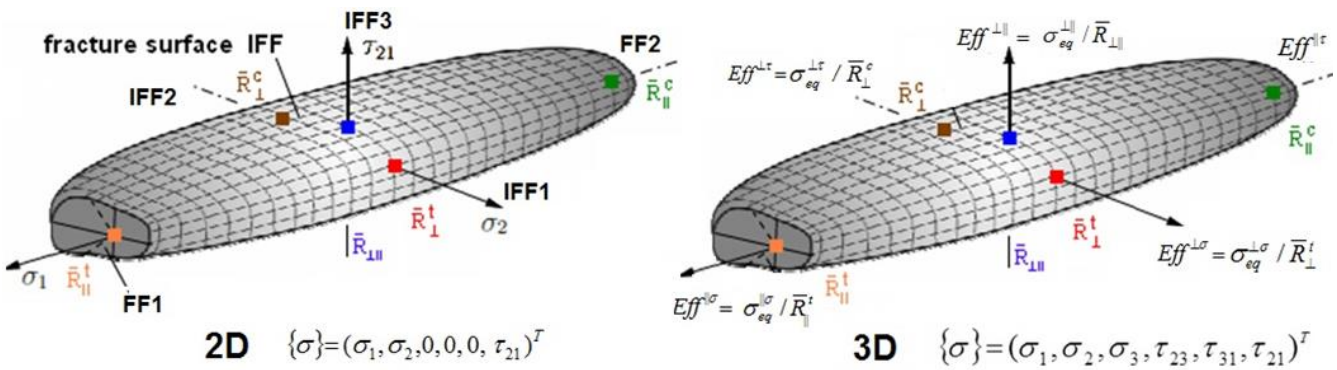

Fig.10: lamina stresses-based surface or fracture body of the UD material and strength-normalized 3D fracture surface [Cun23a, Cun13]

In thin laminas at maximum 3 modes of the 5 modes will physically interact. Considering layers within 3D-loaded thick laminates, here all 3 IFF modes might interact. Again, the value of the interaction exponent *m* is obtained by curve fitting of test data in the transition zones. For *m*, also termed rounding-off exponent, the size of which is high in case of low scatter and vice versa. A lower value chosen is more on the 'safe' side.
Of interest is not only the interaction in the mixed failure domains or interaction zones of adjacent failure modes, respectively, but further the joint failure in a multi-fold failure domain (superscript $^{\mathrm{MfFD}}$) such as in the $(\sigma_2^t,\ \sigma_3^t)$-domain. See the mapping of this failure effect in the *Table 4*, before, or how a twofold mode stress effort acts is captured.

4.4 Orthotropic Fabric Material

NCF are composed of UD laminas which can usually be computed and modelled without any major difficulties by the CLT as long as the reinforcing stitch thread with its stitch thread volume content, stitch density and thread diameter are practically not leading from the 2D material to a real 3D-material. If the NCF composites have a polymeric stitch thread which smelts during manufacturing, then CLT-based predictions are best.

Woven fabrics require more 'homogenizing work' than Non-crimp fabrics (NCF).

4.4.1 2D-modelling of a Woven 2D-NCF-fabric reinforcement

Fig.11 visualizes a possibility to model a fabric by basic equivalent UD layers. This is not optimal for the ratio 1:1 or binding pattern of the plain weave (*German: Leinwand*) but may be sufficient for the 1:8 binding pattern (satin weave, Atlas).

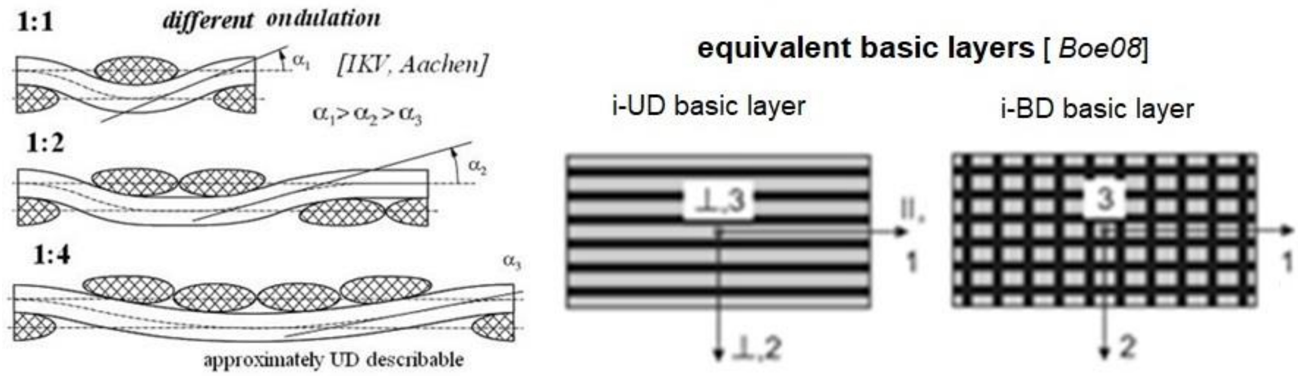

Fig.11: 2D-Modelling of differently woven fabrics with basic layers

In this context, if the CLT for laminates, composed of UD laminas, could be also applied to textile-reinforced composites, the following steps need to be undertaken, see [*Böh08*]: (1) Theoretical decomposition of the textile composites into idealized UD laminas, i-UD layers, (2) Evaluation of experimentally determined stress-strain curves in different directions of the textile-reinforced composite, and 3) Identification of the engineering constants of the i-UD layer by inverse identification or by numerical analysis.
It has to be stated that the reverse identification of engineering constants for i-UD layers of woven composites is not always possible especially when the warp/fill fibre content is not 1:1 (e.g. for an atlas 1:4 reinforcement). Furthermore, research has shown that the reverse identification could lead to too high engineering constants so that the theoretically obtained stress-strain response of the woven composite is usually overestimated. To overcome this drawback, several researchers proposed so-called textile-specific correction factors. All engineering constants are multiplied with these factors in order to consider the influence of fibre undulations etc on the engineering constants, [*Böh08*]

Fig.12 collects properties and 3D-stresses in the fabric material CoS.

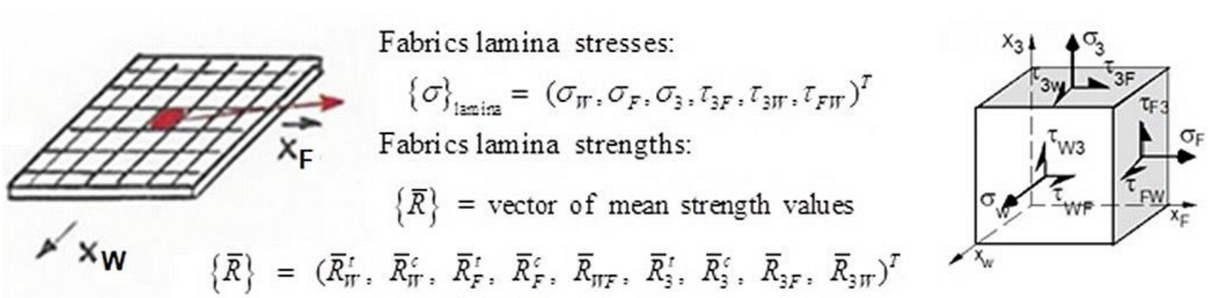

$$\{E\} = (E_{||}, E_{\perp}, G_{\perp||}, G_{\perp\perp}, \nu_{\perp||})^T \text{ with } \nu_{\perp\perp}, \nu_{\perp||} \text{ off-diagonal, and } G_{\perp\perp} = E_{\perp} / (2 + 2 \cdot \nu_{\perp\perp})$$

Fig.12: Properties and stresses of the fabric material [Cun98]

4.4.2 2D- and 3D-SFCs of the Orthotropic Fabric

The following table, *Table 5*, includes the FMC-based SFCs for the porous orthotropic (rhombic-anisotropic) fabric ceramic material.

Table 5: 3D-SFC formulations for 'porous' 2D-woven fabric materials

Fabric invariants, privately obtained from J.F. Boehler, 1995

$$I_1 = \sigma_W,\ I_2 = \sigma_F,\ I_3 = \sigma_3,\ I_4 = \tau_{3F}{}^2,\ I_5 = \tau_{3W}{}^2,\ I_6 = \tau_{WF}{}^2,\ I_7 = \tau_{3F}\cdot\tau_{3W}\cdot\tau_{WF}.$$

The derived invariant SFC formulations are:

$$F_W^t = I_1 / R_W^t,\quad F_F^t = I_1 / R_F^t,\quad F_3^t = I_3 / R_3^t,\quad F_W^c = I_1 / R_W^c,\quad F_F^c = I_1 / R_F^c\ ,\ F_3^c = I_3 / R_3^c\ ,$$

$$F_{WF} = I_6 / (R_{WF} - \mu_{WF}(\sigma_W + \sigma_F)),\ F_{3F}^c = \sqrt{I_4} / (R_{3F} - \mu_3\cdot\sigma_3)\ ,\ F_{3W}^c = \sqrt{I_4} / (R_{3W} - \mu_3\cdot\sigma_W)$$

For the insertion into the interaction equation $Eff = 1$ the Eff^{modes} must be provided.

Replacing the invariants by the associated stresses and solving for the Eff^{modes} the author's former 3D-SFC set read

$$\left(\frac{\sigma_W + |\sigma_W|}{2\cdot\bar{R}_W^t}\right)^m + \left(-\frac{\sigma_W + |\sigma_W|}{2\cdot\bar{R}_W^c}\right)^m + \left(\frac{\sigma_F + |\sigma_F|}{2\cdot\bar{R}_F^t}\right)^m + \left(\frac{-\sigma_F + |\sigma_F|}{2\cdot\bar{R}_F^c}\right)^m +$$

$$+\left(\frac{|\tau_{WF}|}{\bar{R}_{WF} - \mu_{WF}\cdot\sigma_W}\right)^m + \left(\frac{|\tau_{WF}|}{\bar{R}_{WF} - \mu_{WF}\cdot\sigma_F}\right)^m +$$

$$+\left(\frac{\sigma_3 + |\sigma_3|}{2\cdot\bar{R}_3^t}\right)^m + \left(\frac{-\sigma_3 + |\sigma_3|}{2\cdot\bar{R}_3^c}\right)^m + \left(\frac{|\tau_{3W}|}{\bar{R}_{3W} - \mu_{3W}\sigma_3^c}\right)^m + \left(\frac{|\tau_{3F}|}{\bar{R}_{3F} - \mu_{3F}\sigma_3^c}\right)^m = 1 = 100\%\ .$$

The equation is engineering-like simplified to just capture the main physics in this interaction equation. It formally considers that there are 2 shear stresses acting at the 2 x 2 sides.

For a cross-ply fabric with Warp = Fill $\rightarrow\ \bar{R}_W^t = \bar{R}_F^t,\ \bar{R}_W^c = \bar{R}_F^c$, the inter-laminar *Eff*s,

suffix $_3$, vanish and just the in-plane (intra-laminar) *Eff*s remain.

The range of parameters is for the interaction-exponent $2.5 < m < 2.9$, and since the strong porosity-dependency very different $\rightarrow$ recommendation: $\mu_{WF} < 0.2\ ,\ \ \mu_3 < 0.2$.

The SFC set above consists of 10 equations which was not in line with Cuntze's 'generic' number 9. An improvement of the friction-effected shear equation parts is to perform by combining two equations. After some discussion Prof. R. Keppeler (*formerly Siemens, now Uni-Bundeswehr Munich.* Thanks Roman) came up with the proposal depicted at the bottom:

For-in-plane stress states the reduced 3D-SFC's set reads:

$$\text{2D:}\ \left(\frac{\sigma_W + |\sigma_W|}{2\cdot\bar{R}_W^t}\right)^m + \left(-\frac{\sigma_W + |\sigma_W|}{2\cdot\bar{R}_W^c}\right)^m + \left(\frac{\sigma_F + |\sigma_F|}{2\cdot\bar{R}_F^t}\right)^m + \left(\frac{-\sigma_F + |\sigma_F|}{2\cdot\bar{R}_F^c}\right)^m + \left(\frac{|\tau_{WF}|}{\bar{R}_{WF} - \mu_{WF}\cdot(\sigma_W + \sigma_F)}\right)^m = 1\,.$$

5 Mapping Application of the SFCs to some available Ceramic Test Data Sets

5.1 Porous Monolithic Model

In *Fig.13* fracture test data of a porous monolithic ceramic material is presented.
Of interest is that the bi-xial strength $\bar{R}^{tt}$ is here higher than the uni-axial tensile strength $\bar{R}^{t}$. For the author. This is an effect of the very complicated measurement of $\bar{R}^{tt}$). Namely, physically it is evident, that a double effect of the internal flaws, pores (*a twofold failure occurrence at* $\sigma_{\mathrm{II}} = \sigma_{\mathrm{III}}$) is acting and this must cause $\bar{R}^{tt} < \bar{R}^{t}$! Also for concrete the same nonsense-result was published [*CUN22,§5.4*]. If the bi-axial strength is not of interest a tension cut-off at $\bar{R}^{t}$ is usually applied.
According to the large scatter the isotropic material-inherent 120°-symmetry, marked by $\Theta \neq 1$, is not considered here. F = 1 ≡ *Eff* = 1 marks the failure envelope.

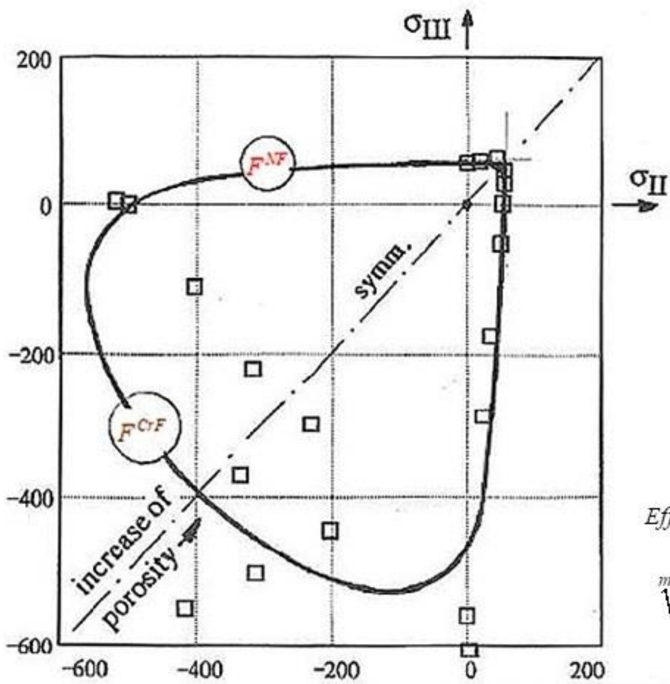

$$\{\bar{R}\} = (\bar{R}^{t}, \bar{R}^{c})^{T} = (60\ ,\ 500)^{T}\,\mathrm{MPa}$$

with μ not to regard here

Normal Fracture NF for $\mathrm{I}_1 > 0$:

$$F^{NF} = c^{NF} \cdot \frac{\sqrt{4J_2 - I_1^2/3} + I_1}{2 \cdot \bar{R}^{t}} = 1$$

Crushing Fracture CrF for $\mathrm{I}_1 < 0$:

$$F^{CrF} = c^{CrF} \cdot \frac{\sqrt{4J_2 - I_1^2/3} + I_1}{2 \cdot \bar{R}^{c}} = 1$$

$$Eff = 1 = \sqrt[m]{\left(c^{NF} \cdot \frac{\sqrt{4J_2 - I_1^2/3} + I_1}{2 \cdot \bar{R}^{t}}\right)^m + \left(c^{CrF} \cdot \frac{\sqrt{4J_2 - I_1^2/3} + I_1}{2 \cdot \bar{R}^{c}}\right)^m}$$

Fig.13: Porous monolithic ceramics [Kow83]. m =2.8, $\sigma^{NF} = 1$

$$I_1 = (\sigma_I + \sigma_{II} + \sigma_{III})\ ,\ \ J_2 = [(\sigma_I - \sigma_{II})^2 + (\sigma_{II} - \sigma_{III})^2 + (\sigma_{III} - \sigma_I)^2]/6$$

The high effect of dfferent porosity is clearly outlined in the graph. The CrF-curve represents as well the mean porosity or 50 %-mean curve.

5.2 UD-Model

Similar to uni-axial and bi-axial reinforced plastic matrices (FRP), for ceramic fibers are produced and collected in a roving and then embedded in the matrix. Compared to monolithic ceramics, fiber-reinforced ceramic components such as silicon carbide fiber-reinforced silicon carbide (SiC/SiC) reduce brittleness, which means it improves damage tolerance by hindering through the fibers the spread of micro-cracks in the matrix. The ceramic fibers are produced from various polymers, so-called precursors, by pyrolysis. The ceramic fibers are divided into oxide and non-oxide fibers (*text derived from* [*Wikipedia*]). *Fig.14* outlines the similarity to FRP-material. The same SFCs are to apply as with UD-FRP regarding the porosity version.

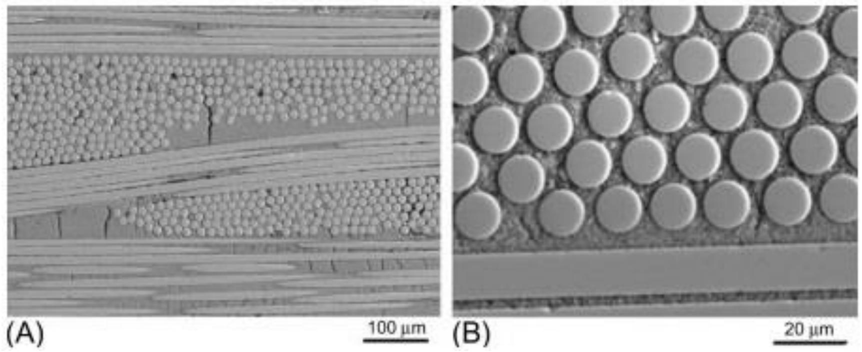

Fig.14. SEM images of Nextel™ 610/mullite composites with 0/90 fiber orientation, (A) fiber bundles and (B) almost regular and dense packing of fibers within a bundle. From Simon, Progress in processing and performance of porous-matrix oxide/oxide composites. Int J Appl Ceram Technol 20052:p.141.

In *Fig.15* for two UD CMCs the failure curve $\tau_{21}(\sigma_2)$ is depicted. This is an Inter Fiber Failure (IFF) mode envelope, a basic cross section of the total *Eff* = 1 = 100% fracture body, see *Fig.11*.

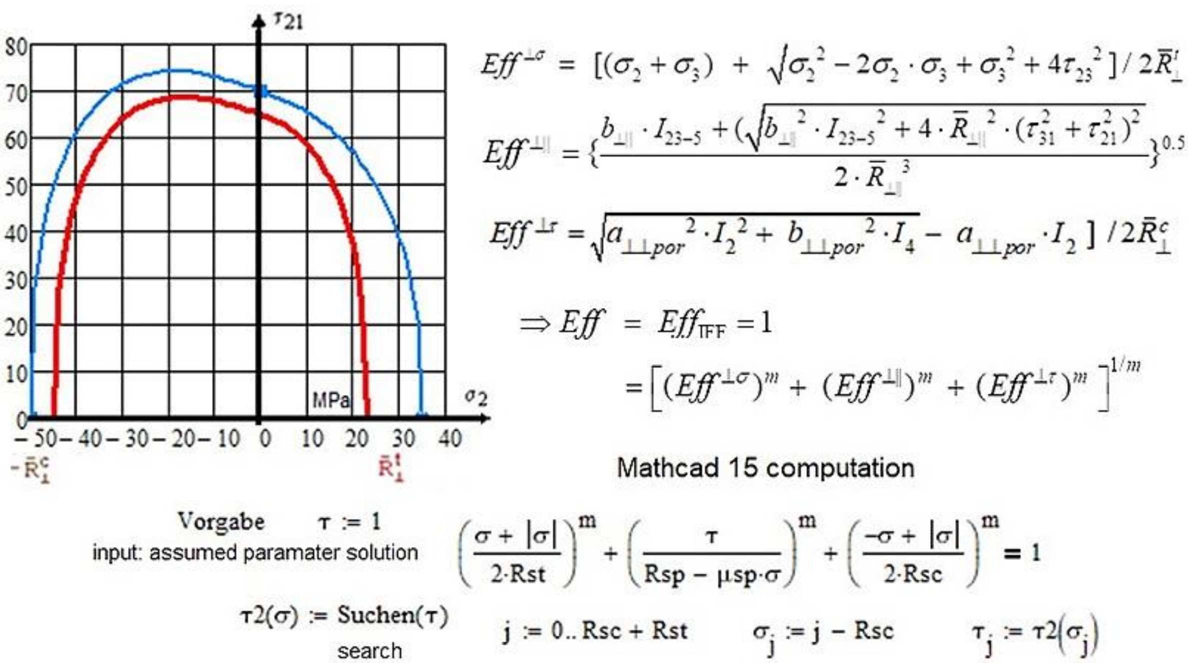

Fig. 15: Failure envelope $\tau_{21}(\sigma_2)$ with SFCs and Mathcad-computation. *Filament wound tube, UD CMC material, WHIPOXTM and C/C-SiC (strength data provided by DLR Stuttgart), [Jai20]. Assumed numbers: * simplified SFC, m = 2.6, μ = 0.35 whereby generally (* $a_{\perp\perp por}(\mu)$, $b_{\perp\perp por}(\mu)$ *).*

WHIPOX-AA-3-45 WOUND HIGHLY POROUS OXIDE CERAMIC MATRIX COMPOSITE: *Fiber Nextel™610 Roving (3000 denier), Matrix Al2O3.*
(down) MathCad 15 calculation with 2D-simplified SCF

The strength properties of the two CMCs are listed below:

$$\text{WHIPOX}^{\text{TM}}:\{\bar{R}\} = (\bar{R}_{\parallel}^{t}, \bar{R}_{\parallel}^{c}, \bar{R}_{\perp}^{t}, \bar{R}_{\perp}^{c}, \bar{R}_{\perp\parallel})^{T} = (279, 243, 22.5, 45, 65)^{T}\ \text{MPa}$$
$$\text{C/C-SiC}\quad :\{\bar{R}\} = (\bar{R}_{\parallel}^{t}, \bar{R}_{\parallel}^{c}, \bar{R}_{\perp}^{t}, \bar{R}_{\perp}^{c}, \bar{R}_{\perp\parallel})^{T} = (190, 170, 35, 50^{*}, 70)^{T}\ \text{MPa} \; .$$

Whipox is a highly porous oxide AllOx material and consists of oxide fibers and an oxide slip-based matrix that is sintered. The material C/C-SiC is produced by liquid silication (LSI). Both materials are manufactured by DLR-Stuttgart.

The associated 2D-failure body would look like the body in *Fig.11*.

Fig.16 presents a bi-axial test data plot of a CMC material from Schunk. In the graph the lower positioned test crosses at about $\sigma_2^c = -7$ MPa cannot stem from an accurate test. Unfortunately, the ILK test team could not sort out whether the reason is the test specimen, the test device or the test evaluation. Decisive for the designer is, that one has to design with practically zero lateral tensile strength $R_{\perp}^{t}$. Of further obvious interest is the UD friction value $\mu_{\perp\parallel}$ for this reinforced ceramic matrix which is much higher than for any reinforced polymer matrix. The material-internal CMC structure seems to cause this high value.

Due to the uncertainty of the measurement in the 'question mark-denoted domain' the author mapped the data set by applying two different friction values.

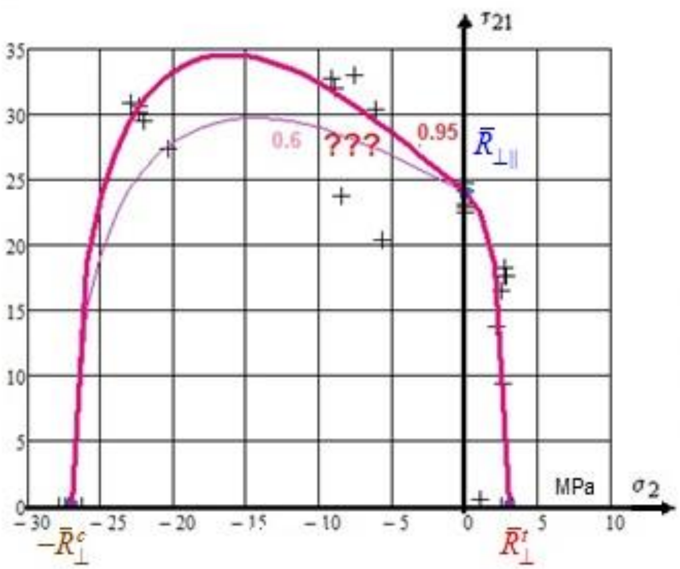

$$\{\bar{R}\} = (-, -, \bar{R}_{\perp}^{t}, \bar{R}_{\perp}^{c}, \bar{R}_{\perp\parallel})^{T}$$
$$= (-, -, 3, 27, 24)^{T}\ \text{MPa}$$
$$\text{with}\ \ \mu_{\perp\parallel} = 0.6,\ 0.95$$

$$Eff_{IFF} = 1 =$$
$$\left(\frac{\sigma_2^{t}}{\bar{R}_2^{t}}\right)^{m} + \left(\frac{-\sigma_2^{c}}{\bar{R}_2^{c}}\right)^{m} + \left(\frac{|\tau_{12}|}{\bar{R}_{\perp\parallel} - \mu_{\perp\parallel}\cdot\sigma_2^{c}}\right)^{m}$$

Fig.16: Failure envelope $\tau_{21}(\sigma_2)$. UD CMC material, 88° tube, test data from Schunk, tested at the ILK Dresden [*Beh18*]*; m =2.6*

5.3 Fabric Model

In the general 3D-case the following set of strength and friction values is to apply:

$$3D: \ \{\bar{R}\} = (\bar{R}_W^t,\ \bar{R}_W^c,\ \bar{R}_F^t,\ \bar{R}_F^c,\ \bar{R}_{WF},\ \bar{R}_3^t,\ \bar{R}_3^c,\ \bar{R}_{3F},\ \bar{R}_{3W})^T \ \text{with} \ \mu_{WF}, \mu_{3W}, \mu_{3F}$$

$$2D, \text{general}: \quad \{\bar{R}\} = (\bar{R}_W^t,\ \bar{R}_W^c,\ \bar{R}_F^t,\ \bar{R}_F^c,\ \bar{R}_{WF})^T \ \text{with} \ \mu_{WF} \ .$$

$$2D,\ W = F, \text{plain weave}: \ \{\bar{R}\} = (\bar{R}_W^t,\ \bar{R}_W^c,\ (\bar{R}_W^t),\ (\bar{R}_W^c),\ \bar{R}_{WF})^T \ \text{with} \ \mu_{WF}$$

The presented test campaign results outline the challenge when testing brittle ceramic. One must always consider that the inherent flaws give rise to micro-mechanical fracture mechanics under tension. This is usually of a less influence for compression.

5.3.1 σ_W (σ_F), bi-axial tension

Fig.17 shows the test results of 8 CMC fabric tube test specimens of a fabric C/SiC.

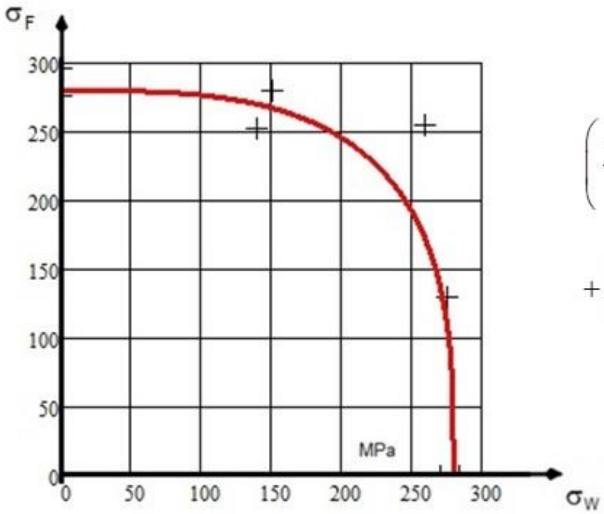

$$\left(\frac{\sigma_W + |\sigma_W|}{2 \cdot \bar{R}_W^t}\right)^m + \left(-\frac{\sigma_W + |\sigma_W|}{2 \cdot \bar{R}_W^c}\right)^m + \left(\frac{\sigma_F + |\sigma_F|}{2 \cdot \bar{R}_F^t}\right)^m + \left(\frac{-\sigma_F + |\sigma_F|}{2 \cdot \bar{R}_F^c}\right)^m = 1$$

Fig.17: Failure envelope σ_W (σ_F). plain weave fabric C/SiC tube for X38 Body Flap, reentry, $\sigma_W(\sigma_F)$ *,*
RT, MAN-Technologie, m =3 , 1997, $\bar{R}_W^t \cong \bar{R}_F^t$ *= 278 MPa, CVI process* [*Cun98, Cun98b*]

5.3.2 τ_{WF} (σ_W), shear stress-normal stress

The next test specimens are cut out of a laminate plate at an angle to the specified 0°- direction angle of the fabric test specimen $\begin{bmatrix} 0 \\ 90 \end{bmatrix}_S$, [*courtesy Siemens AG*]. For in-plane stressing of this off-axis test specimen, the following SFC set remains:

$$2D: \ \left(\frac{\sigma_W + |\sigma_W|}{2 \cdot \bar{R}_W^t}\right)^m + \left(-\frac{\sigma_W + |\sigma_W|}{2 \cdot \bar{R}_W^c}\right)^m + \left(\frac{\sigma_F + |\sigma_F|}{2 \cdot \bar{R}_F^t}\right)^m + \left(\frac{-\sigma_F + |\sigma_F|}{2 \cdot \bar{R}_F^c}\right)^m + \left(\frac{|\tau_{WF}|}{\bar{R}_{WF} - \mu_{WF} \cdot (\sigma_W + \sigma_F)}\right)^m = 1 \ .$$

In uniaxial stress states $\sigma_W{}^c$ (*Warp stability danger faced, same is valid for the Fill direction*) and $\sigma_W{}^t$ fiber failure modes are identified in the case of plain weave fabrics. Under τ_{WF}, accompanied by scissoring, micro-mechanical matrix failure may be faced in off-axis testing. This is of marginal importance for $\tau_{WF}(\sigma_W{}^c)$ but essential for $\tau_{WF}(\sigma_W{}^t)$. Namely, at small tensile warp stresses fracture danger for the matrix (index *m*) due to σ_m^t under shear stresses τ_{WF} is given through the matrix tensile fracture-causing tensile component of the shear stress, $\tau_{WF} \equiv (\sigma_m^c, \sigma_m^t)$. This lasts until fiber tensile failure stress $\sigma_W{}^t \equiv \sigma_{||}{}^t$ dominates the failure state.

Matrix tensile fracture leads to an inward dent as logical consequence, see *Fig.18*. However, why is a dent to face there, represented by the two circle-marked test points? The inward dent or pop-in is just the consequence of the off-axis angle test specimen, which activates matrix failure in this not adequate $\tau_{WF}(\sigma_W^{\ t})$ -test. In the so-called off-axis coupons, a tensile stress-controlled matrix break is generated from about 15° on. The fibers are no longer continuous over the test length, which means that the matrix is practically the highest stressed constituent. To capture this effect would require a matrix constituent strength criterion. A smeared composite criterion cannot deliver this. ► The two cross-marked test data points are just the consequence of the not fully suitable test specimen.

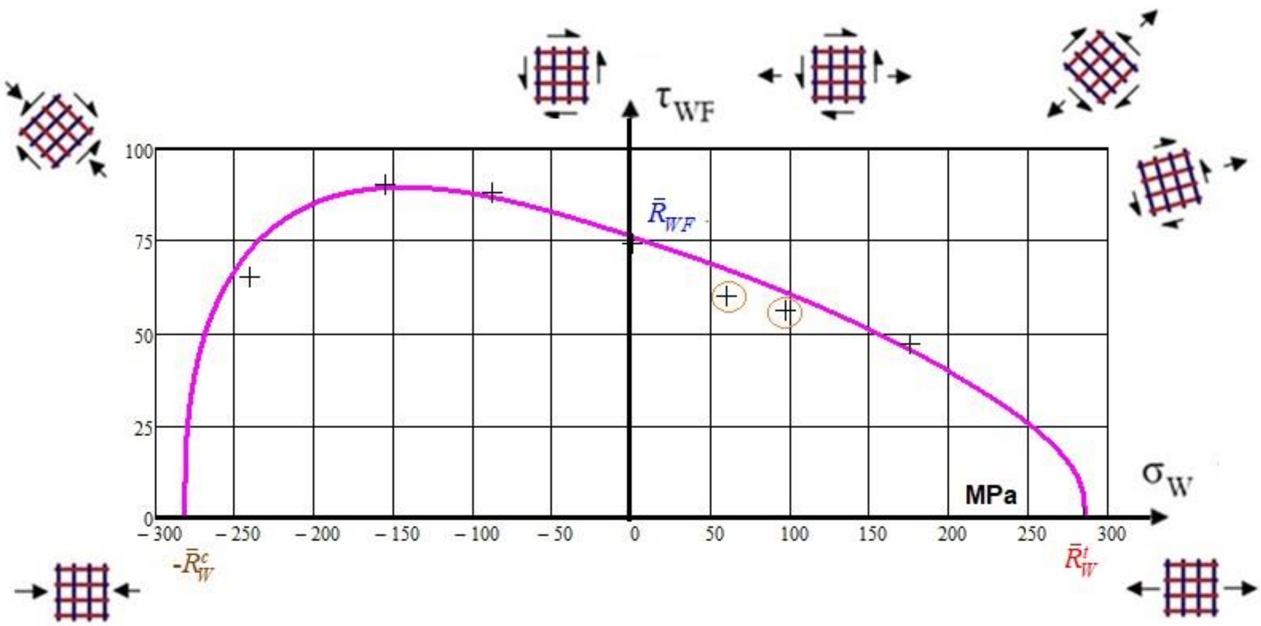

Fig. 18: Off-axis coupon tests, $\begin{bmatrix} 0 \\ 90 \end{bmatrix}_S$ *Failure envelope* $\tau_{WF}(\sigma_W)$. *(data set Siemens AG). m =* ***2.6***

Plain weave fabric laminate. RT=23°C. From mapping derived strength values. $R_W^{\ t}$ *= 286 MPa,* $R_W^{\ c}$ *= 282 MPa. Josipecu shear test* R_{WF} *= 76 MPa,* μ_{WF} *= 0.14*

(If a mapping of the dent would be really desired: A numerical solution to map the dent would be to move from the shear mode at α = 15° to a matrix tensile mode and about 50° from the matrix tensile mode back to the warp tensile mode. This requires the formulation of a matrix failure mode. Built on practical experience a decay function is to employ. This decay function for each interacting mode is physically accurately terminated in each opposite 'pure' domain τ_{WF} and $\sigma_W^{\ t}$).

<u>Lessons Learned from testing</u>:

* The transfer of test results from the test specimen to the real part requires deep insight! One must know the characteristics of the test specimen before transferring properties to the structural part

*Application limit of the usually and here applied series spring model is given if abrupt changes of a mode are faced. An inward dent cannot be mapped since this violates the basis of the series failure model used in the FMC-based Cuntze SFCs , however also in each other SFC

* Each test method has its application limit. Not plausible test points have to be checked by physical interpretation

* The dent is an off-axis coupon-caused result and does not reflect a real macro-scopic $\tau_{WF}(\sigma_W{}^t)$ -failure curve

* The hinge or increase of the shear failure curve in the negative σ_2-domain – indicated by an increasing shear stress – is not caused by an increase of the (*uni-axial*) shear 'strength'. *Eff* remains constant, Mohr-Coulomb just improves the bi-axial 'strength *capacity*' and not the technical strength

* Uncover the reasons of large scatter

* In the case of very large scatter, mapping of the course of test data points with a SCF model makes no much sense and might partly also not be possible. Also a strength design value *R* cannot be determined or would mathematically result in a reduced strength value of practically zero

*A validated SFC model cannot model physically false test points, but the other way round, it can help to sort out bad measurements or physically doubtful test values

* Correct loading can be practically only applied to a straight edge

* From bad experience of the author, when interpreting CMC-test results: A figure capture must indicate whether it is a UD ply or a fabric ply or something else??

Here the saying fits:

"***Well-understood experiments have to verify the design assumptions made***"!

In this context Avula stated in 1987 "Experimental observations and measurements are generally accepted to constitute the backbone of physical sciences and engineering because of the physical insight they offer to the scientist for formulating the theory. Concepts, which are developed from observation, are used as guides for the design of new experiments, which in turn are used for validation of the theory. Thus, experiments and theory have a hand-in-hand relationship".

5.3.3 Some further test results with mapping

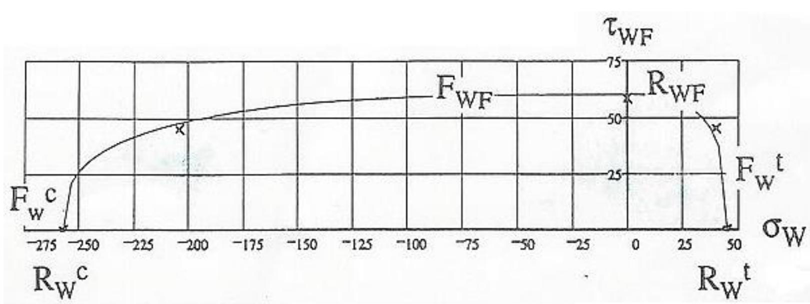

Fig. 19: Failure envelope $\tau_{WF}(\sigma_W)$,C/C-SiC tube, T =1600°C, m = 3 [Gei97].

$$\{\bar{R}\} = (\bar{R}_W^t,\ \bar{R}_W^c,\ \bar{R}_F^t,\ \bar{R}_F^c,\ \bar{R}_{WF},\ \bar{R}_3^t,\ \bar{R}_3^c,\ \bar{R}_{3F},\ \bar{R}_{3W})^T = (45,\ 260,\ -,\ -,\ 59,\ -,\ -,\ -,\ -)^T \text{ MPa}$$

-

The course in the domain $\sigma_W{}^c, \tau_{WF}$ seems to contradict to *Fig. 18*, however, the materials are different and the quality of the distribution of the provided test points is not comparable.

The fabric *Fig.20* presents a spatial envelope with also here too few test points.

$$\left(\frac{\sigma_3 + |\sigma_3|}{2 \cdot \bar{R}_3^t}\right)^m + \left(\frac{-\sigma_3 + |\sigma_3|}{2 \cdot \bar{R}_3^c}\right)^m + \left(\frac{|\tau_{3F}|}{\bar{R}_{3F} - \mu_{3F}\sigma_3^c}\right)^m = 1$$

$$\{\bar{R}\} = (\bar{R}_W^t,\ \bar{R}_W^c,\ \bar{R}_F^t,\ \bar{R}_F^c,\ \bar{R}_{WF},\ \bar{R}_3^t,\ \bar{R}_3^c,\ \bar{R}_{3F},\ \bar{R}_{3W})^T$$
$$\bar{R}_W^t,\ \bar{R}_W^c,\ \bar{R}_F^t,\ \bar{R}_F^c,\ \bar{R}_{WF},\ 3,\ 99,\ 7,\ \bar{R}_{3W})^T$$

with $\mu_{WF}, \mu_{3W,} \mu_{3F} = 0.3$

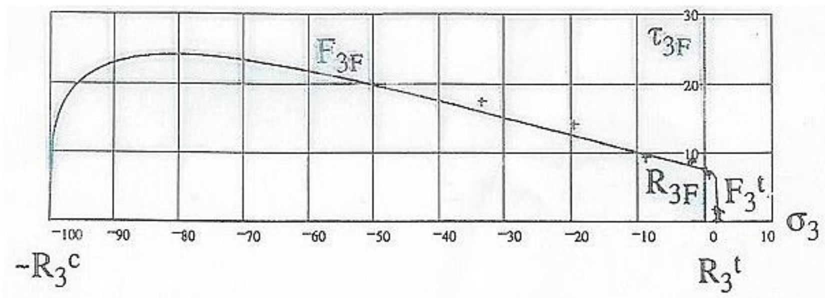

Fig. 20: Failure envelope $\sigma_W(\sigma_F)$,C/SiC tube, RT, m =3,

(test data from dissertation B. Thielicke, 1997) {Thi97[

6 Conclusions & Outlook

6.1 General Conclusions on the Author's FMC-based SFCs

- The presented invariant-based (*invariants have the advantage that the transfer between coordinate systems is automatically given)* 3D-SFC sets are physically-based due to the choice of physically meaningful invariants linked to the solid-behavior together and consideration of the fulfillment of the material-symmetry demands
- FMC-based 'modal' SFCs are simple but describe physics of each separately mapped failure mechanism of the 3 different material families pretty well, see the papers of the author [*Cun08, Cun17, CUN22*]. They deliver a combined formulation of independent modal failure modes, without facing the shortcomings of 'global' SFC formulations, which mathematically map *in-dependent* failure modes
- Clear equivalent stresses can be calculated for the provided 'modal' SFCs
- The size of each Eff^{mode} informs the designing engineer about a mode's failure importance thereby outlining the design-driving mode
- Similarly behaving materials possess the same shape of a fracture body and use the same SFC
- Model parameters are just the measurable technical strengths *R* and friction value μ, and on top the interaction exponent *m*. The determination of μ comes from mapping the compression stress-shear stress domain and of *m* by mapping the transition zone between the modes. A good guess is m = 2.6 for all mode transition domains and all material families
- A usual SFC just describes a 1-fold occurring failure mode or mechanism! A multi-fold occurrence of the same failure mode with its joint probabilistic failure effect is additionally to be considered in each formulated modal SFC. Traditional global SFCs do not capture this effect and thus violate for instance in the case of isotropic materials the isotropy-inherent 120°-symmetry of the failure body
- Using *Eff* excellently supports 'Understanding the multi-axial strength capacity of materials'. For instance, 3D-compression stress states have a higher bearing capacity, but the value of *Eff* nevertheless stays at 100%. Consequently, this has nothing to do with an increase of a (*uniaxial*) technical strength *R* which is a fixed result of a Standard! The following fracture test result of a brittle concrete impressively shows how a slight hydrostatic pressure of 6 MPa increases the strength capacity in the longitudinal axis from 160 MPa up to 230 MPa - 6 MPa = 224 MPa. Therefore, the benefit of 3D-SFCs–application could be proven as the fracture stress states below depict:

  $$\sigma_{\text{fr}} = (\sigma_I\,,\ \sigma_{II}\,,\ \sigma_{III}\,)_{\text{fr}}^{\text{T}} = (-160,\ 0,\ 0)^{\text{T}}\,\text{MPa} \Leftrightarrow (-224-6,\ -6,\ -6)^{\text{T}}\,\text{MPa}.$$

  Both the *Eff*s = 100% for $(-160,\ 0,\ 0)^T$ and for $(-224-6,\ -6,\ -6)^T$ in [*CUN5.5*]!

  This could be partly transferred to the quasi-isotropic plane of the transversely-isotropic CMC-UD-material, $\sigma_2 - \sigma_3$, and to the orthotropic CMC fabric, when beside shear τ_{WF} the compressive stress σ_W^c acts together with σ_F^c and both activate friction on the sides.

Application hint to sensitize the designer:
Most of the CMC materials, due to the porosity, are very sensitive to shear stress in the direction of the shell's thickness, which is always the case, for example, at support points. The same is valid for local normal loading on the shell.

Mind, please:
* Above CMC-materials can be treated by the Classical Laminate Theory (CLT)
* Braided composites are not investigated here. Their numerical modelling usually applies meso-scale (between micro-scale and macro-scale) unit cell FE models to study the material behavior.
* Both, a growing yield surface (ductile material) and a growing micro-damage surface (brittle material) are terminated by a fracture failure surface.

6.2 Validation of Ceramic SFC-Models

Validation of the lamina (layer or ply) model is achieved if the mapping of the course of the failure stress point (*strength resistance test data*) is good. This means that the uncertainty of the scattering resistance properties is captured by (P = 50%, C= 50%) with P the survival probability and C the confidence level applied when estimating a basic population value from sample test data sets. Regarding Mohr-Coulomb, an accounting for friction value effects is mandatory. because compression and shear (*shear constituent compression stress*) are generally act.
Modelling the courses of test points leads to an average failure curve or body. This requires the use of average strengths $\bar{R}$ and an average value (statistical mean) for each required friction value μ. For the strengths, the confidence level C is considered as a one-sided tolerance level. Average values are applied in order to achieve the best expectation behavior of the structural part.

The application of a SFC It is to pay attention with the in the case of micro-failure modes of constituents of the homogenized (*smeared*) material. Therefore, High Fidelity macro-mechanical strength criteria should always 'consider' non-separable micro-mechanical failure effects. For instance, a bi-axially stressed UD bar may tension fail under lateral biaxial compression without any external axial loading.

Shortcomings of inclined (*off-axis*) coupon tests, for instance, explained by a matrix failure, have nothing to do with the macro-scopic material model.

The provided SFC sets for the 3 CMC model families could just successfully applied to a small number of available test data sets. For his set of 5 UD failure criteria Cuntze needs for spatial stress cases 7 measurable model parameters (5 strengths + 2 friction values) and from experience a definable interaction exponent *m*.

Delamination is not a failure of the lamina but of the 'structure' laminate. At the coupon edges it is termed edge effect. Within the laminate, delamination can be predicted by the application of the inter-laminar stresses-associated 3D-SFCs (*just suffix 3 parts*). At the edges it is - due to the stress singularity – a task of fracture mechanics tools to predict debonding using a Cohesive Zone model or Finite Fracture Mechanics [*Met23*].

6.3 Design Verification

A simulation process, considering the basic loadings, requires the performance of many analyses in order to optimally simulate the structural component's behavior to finally achieve a suitable design parameter set for Design Dimensioning. This set describes the average behavior well and should fit the structural test results and this set enables to build a prototype but not to build a safety-critical structural component. For them, in the Design Verification (DV) a statistically based approach with a minimum number of measurable design parameters is mandatory. Classically, a Safety Concept is given with Design Factors of Safety j based on long term experience and finally a positive Reserve Factor RF is to demonstrate. The purpose of the design FoS j is to guaranty quality of the design in order to achieve a certain level of Structural Reliability for the hardware. Different industry has different risk acceptance attitudes and applies differently high FoS values!

As the procedure is the same a guiding numerical DV example is taken from a UD-fiber-reinforced plastic material**):** For obtaining DV at first a statistical reduction of the average strength defined by (P = 50%, C = **50**%) down to e.g. (P = 90% or 95% (A-value), C = **95**%) is performed. This reduction procedure $\{\bar{R}\} \rightarrow \{R\}$ helps to keep the generally accepted structural reliability of about $\Re = 1 - p_f > 1 - 10^{-7}$, denoting p_f the failure probability.

Asssumption: Linear analysis permitted, design FoS $j_{\text{ult}} = 1.25$

* Design loading (action): $\{\sigma\}_{\text{design}} = \{\sigma\} \cdot j_{\text{ult}}$

* 2D-stress state: $\{\sigma\}_{\text{design}} = (\sigma_1, \sigma_2, \sigma_3, \tau_{23}, \tau_{31}, \tau_{21})^T \cdot j_{\text{ult}} = (0,\ -76,\ 0,\ 0,\ 0,\ 52)^T \text{MPa}$

* Residual stresses: $0\ \left(\textit{effect vanishes with increasing micro-cracking}\right)$

* Strengths (resistance) : $\{\bar{R}\} = (1378,\ 950,\ 40,\ 125,\ 97)^T \text{MPa}$ average from mesurement

statistically reduced $\{R\} = (R_{||}^t, R_{||}^c, R_{\perp}^t, R_{\perp}^c, R_{\perp||})^T = (1050,\ 725,\ 32,\ 112,\ 79)^T \text{MPa}$

* Friction value(s) : $\mu_{\perp||} = 0.3,\ (\mu_{\perp\perp} = 0.35)$, Mode interaction exponent: $m = 2.7$

$$\{Eff^{\text{mode}}\} = \left(Eff^{||\sigma},\ Eff^{||\tau},\ Eff^{\perp\sigma},\ Eff^{\perp\tau},\ Eff^{\perp||}\right)^T = \left(0.88,\ 0,\ 0,\ 0.21,\ 0.20\right)^T$$

$$Eff^m = (Eff^{||\sigma})^m + (Eff^{||\tau})^m + (Eff^{\perp\sigma})^m + (Eff^{\perp\tau})^m + (Eff^{\perp||})^m = 100\% \ .$$

The results above deliver the following material reserve factor $f_{\text{RF}} = 1 / Eff$

$$* \ Eff^{\perp\sigma} = \frac{\sigma_2 + |\sigma_2|}{2 \cdot \bar{R}_{\perp}^t} = 0, \quad Eff^{\perp\tau} = \frac{-\sigma_2 + |\sigma_2|}{2 \cdot \bar{R}_{\perp}^c} = 0.60, \quad Eff^{\perp||} = \frac{|\tau_{21}|}{\bar{R}_{\perp||} - \mu_{\perp||} \cdot \sigma_2} = 0.55$$

$$Eff = [(Eff^{\perp\sigma})^m + (Eff^{\perp\tau})^m + (Eff^{\perp||})^m]^{1/m} = 0.80.$$

$$\Rightarrow \quad f_{\text{RF}} = 1 / Eff = 1.25 \rightarrow \text{RF} = f_{\text{RF}} \text{(if linearity permitted)} \rightarrow \text{MoS} = RF - 1 = 0.25 > 0 \ !$$

The certification–relevant load-defined Reserve Factor RF corresponds in the linear case to the material reserve factor f_{RF}. It's value here is 1.25 > 1 and therefore → Laminate wall design is verified!

High scatter means high uncertainty and automatically will exclude the use of such a material from application, regarding the statistically reduced low design strength. Scatter matters more than the average value in Design Verification.

Note on the application of Continuum micro-Damage Mechanics (CDM):

In literature. i.e. [*Jai20*], Continuum (micro-)Damage Mechanics (CDM) models are also used to determine a *RF*. Analogous to the standard procedure then statistically-based micro-damage model parameters are required and a maximum value *D* is to define according to $D < D_{admissible} < 100\%$ at failure (must be statistically based). Defining such a *D*–value is a challenge for the application of (micro-)Damage Models in the mandatory DV for serial production certification. This challenge is higher than for providing the classical strength design allowables *R*.

Further, it in the standard procedure it runs $0 < Eff < 100\%$, whereas *D* begins at a distinct *Eff*-value but should principally also end at 100%, see [*CUN22,§15.3*]. How does the designer assess a stress level that is below the onset-of-micro-damage? In this context exemplarily the question arises: How are to consider stresses in Low Cycle Fatigue.

Stiffness decay CDM model parameters are difficult to apply. The provision of a CDM-failure surface analogous to for instance *Fig.11* would be mandatory for DV. Hence, up to now CDM seems not to meet the authority-demanded DV-requirements regarding the statistically reduced design strength *R* and regarding the relationship $\sigma \sim R \cdot Eff$.

7 Literature

[Beh18] Behnisch, T: *Zum Einfluss querdruckinduzierter Schädigung auf die mechanischen Eigenschaften von Textilverbundkeramiken*. Dissertation 2018, ILK , TU-Dresden

[Boe08] Böhm R: *Bruchmodebezogene Beschreibung des Degradationsverhaltens textilverstärkter Verbundwerkstoffe*. Dissertation, TU Dresden, 2008

[Cha77] Chamis C C and Sinclair J H: *Ten Deg Off-Axis Test for Shear Properties in Fiber Composites*. NASA Lewis research Center, Doc ID 19770016264

[Cun98] Cuntze R: *Strength Prediction for Multi-axially Loaded CMC-Materials*. 3rd European Workshop on thermal Protection Systems. ESA-ESTEC: Noordwijk, March 1998, WP P141

[Cun98b] Cuntze R: *Application of 3D-strength criteria, based on the so-called "Failure Mode Concept", to multi-axial test data of sandwich foam, concrete, epoxy, CFRP-UD lamina, CMC-Fabric Lamina*. ICCE/5, Las Vegas, July 1998 (presentation)

[Cun08] Cuntze R.: *Strength Failure Conditions of the Various Structural Materials: Is there some Common Basis existing*?. SDHM, vol.074, no.1, pp.1-19, 2008

[Cun13] Cuntze R: *Comparison between Experimental and Theoretical Results using Cuntze's Failure Mode Concept model for Composites under Tri-axial Loadings* – Part B of the WWFE-II. Journal of Composite Materials, Vol.47 (2013), 893-924

[Cun17] Cuntze R: *Fracture Failure Bodies of Porous Concrete (foam-like), Normal Concrete, Ultra-High-Performance-Concrete and of the Lamella - generated on basis of Cuntze's Failure-Mode-Concept (FMC*). NWC2017, June 11-14, NAFEMS, Stockholm*

[CUN22] *Life-Work Cuntze - a compilation*. 2023. The Failure-Mode-Concept FMC, a physical and theoretical Material Symmetry-driven basis to generate Strength Criteria, that gave a reason to look after a 'more closed' Strength Mechanics Building & in addition Very Much on Structural Materials, Techniques and Design including work-life experience of the author in many engineering fields (about 850 pages). downloadable from https://www.carbon-connected.de/Group/Prof.Ralf.Cuntze

[Cun23a] *Design of Composites using Failure-Mode-Concept-based tools - from Failure Model Validation to Design Verification.* Mechanics of Composite Materials, Vol. 59, No. 2, May, 2023, pp. 263-282 *

[Cun23b] *Minimum Test Effort-based Derivation of Constant-Fatigue-Life curves - displayed for the brittle UD composite materials.* Springer, Advanced Structured Materials, Vol.199, 107 – 146. in *

[Cun23c] *Comparative Characterization of Four Significant UD Strength Failure Criteria (SFC) with focusing a direct use of Friction Values, use of 'Strength' and 'Proportional Loading'. 54 pages**

[Gei97] Geiwitz W, Theuer A and Ahrends F J: *Experimentelle Bestimmung eines Versagenskriteriums für faserverstärkte Keramik*. Tagungsband "Verbundwerkstoffe und Werkstoffverbunde", Kaiserslautern, September 1997

[Jai20] Jain N and Koch D: *Prediction of Failure in Ceramic Matrix Composites Using Damage-Based Failure Criterion*. J. Compos. Sci. 2020, 4, 183; doi:10.3390/jcs4040183

[Kow83] Kowaltschuk B.I. and Giginjak F.F.: *Monolithic ceramic tests* ... .; in Russian, Kiew, Naikowa Dumka 1983

[Kum02] Kumosa M, Odegard G, Armentrout D, Kumosa L, Searles K and Sutter J K: *Comparison of the ±45°Tensile and Josipecu Shear Tests for Woven Fabric Composite Materials*. J. of Composites Technology and Research, Jan 2002

[Met23] Methfessel T S and Becker W: *Debonding prediction of a reinforcing CFRP patch (better strip) on concrete structures*. CICE 11th Int. Conf. on FRP Composites in Civil Engineering. July 2023, Rio. FSM Darmstadt, 17 pages

[Pet15] Petersen E, Cuntze R and Huehne C: *Experimental Determination of Material Parameters in Cuntze's Failure-Mode-Concept-based UD Strength Failure Conditions*. Composite Science and Technology 134, (2016), 12-25*

[Sch23] Schneller A: *CMC under the aspect of sustainability and resource efficiency*. Presentation WG Sustainability-Kick off, 29th June 2023

[Thi07] Thielicke B: *Die Ermittlung der interlaminaren Scherfestigkeit von kohlenstoff-faserverstärkten Kohlenstoffen mit dem Druckscherversuch im Temperaturbereich zwischen Raumtemperatur und 2000°C*. Dissertation, Uni Karlsruhe, 1997

[VDI06] VDI 2014, *German Guideline*, *Sheet 3*, *Development of Fibre-Reinforced Plastic Components*, *Analysis*. Beuth-Verlag, 2006 (in German and English, author Cuntze was convenor, editor and co-author.

Acknowledgement:

This single authored, non-funded investigation transfers the results of the author's FMC-based SFCs for polymeric matrices to the fully brittle CMC materials where the author's experience is some twenty years old. Therefore, the author is very grateful to have gotten support from Prof. Dr.-Ing. R. Keppeler (*formerly Siemens AG*) and from Dr.-Ing. T. Steinkopf (Siemens) and especially for a highly welcomed CMC fabric data set from Siemens. Also the comments of Prof. Dr. Dietmar Koch, MRM Uni Augsburg, are highly appreciated